Design of a radio-frequency facing-target sputtering system for low-damage thin film deposition

by

Sophia Weeks

Submitted to the Department of Physics
in partial fulfillment of the requirements for the degree of

Bachelors of Arts

at

Mount Holyoke College

May 2013

Author . . . .
Department of Physics
May 10, 2013

Certified by . . . .
Alexi C. Arango
Assistant Professor of Physics
Thesis Supervisor

Accepted by . . . .
Katherine Aidala
Chair, Department of Physics

Design of a radio-frequency facing-target sputtering system for low-damage thin film deposition

by

Sophia Weeks

Submitted to the Department of Physics
on May 10, 2013, in partial fulfillment of the
requirements for the degree of
Bachelors of Arts

Abstract

Thin film devices are becoming increasingly important in the electronic semiconductor industry. For example, organic light-emitting diodes provide many advantages for the development of flat panel displays used in mobile phones, while thin film transistors have provided solutions in the fabrication of OLED backplanes. Organic photovoltaics have the potential to provide our planet with a vast supply of clean, cheap energy.

Thin film deposition processes today have a number of drawbacks, including complicated and time-consuming operation procedures, high cost of construction, and laborious maintenance procedures. While these methods are currently being used effectively in premier research laboratories, addressing these problems would open up the field to researchers with less time and fewer resources.

For this purpose, we have designed and constructed a state-of the art thermal evaporator which is inexpensive, simple and quick to operate, and easy to maintain. While common thermal evaporators are situated inside the glove box, the evaporator developed in this project is mounted instead beneath the glove box floor with top-loading substrate access from inside the glove box. A retractable base plate elevator system enables access to the chamber from outside the glove box through the chamber floor. These improvements maximize space inside the glove box and accessibility of the evaporator chamber, and the chamber's compact size significantly reduces construction costs and pump-down times.

We have also designed a radio-frequency facing-target magnetron sputtering system, which shares these features. However, current sputter deposition processes face additional problems. The fabrication of many semiconductor devices involves deposition onto a substrate previously coated with an organic

thin film. Energetic particles in the sputtering plasma have been shown to cause critical damage to underlying organic layers on substrates during sputter deposition. Consequently, our sputtering system takes advantage of the facing target configuration, which has been shown to effectively confine the sputtering plasma below the substrates, thereby protecting previously deposited organic layers. The design also features high strength magnets positioned above the sputter guns to create a high magnitude magnetic field near the substrates for further protection from high energy electrons and ions. Radio frequency excitation of the sputtering plasma allows for the deposition of insulating materials.

CAD designs for both the evaporator and the sputtering system were created in SolidWorks, and Finite Element Analysis (FEA) was performed using Maxwell 3D. The evaporator has been built and is operating smoothly with no user errors. The total cost was under $40K. The chamber takes less than 3 minutes to pump down, while deposition takes less than 10 minutes. Cleaning is as easy as switching out the metal sleeve, which takes 15 minutes at most.

Thesis Supervisor: Alexi C. Arango
Title: Assistant Professor of Physics

Acknowledgments

I would like to thank the following for their help and support in completing this project:

- My adviser, Professor Alexi Arango, for giving me the opportunity to pursue my interests in engineering and computer aided design. His enthusiasm for solar energy and determination to change national energy standards kept me excited about research and motivated me when I might have given up.

- Professor Spencer Smith for being part of my thesis committee, as well as being a fun and engaging lab instructor to work with as a teaching assistant.

- Professor Lee Bowie for being part of my thesis committee, as well as introducing me to the wonders of Gödel's Theorem.

- Thomas Liimatainen for machining most of the evaporator components, as well as cheerfully discussing design considerations with me and fixing my bike.

- Leonard McEachern for helping me out in the lab practically every day during the summer. He also had a hand in fixing my bike.

- Maggie Stevens and Phoebe Tengdin, who both worked with me as lab partners at different times in my Arango lab career and helped me build my first solar cells.

- Emily Tansey and Shehzeen Hussain for testing my solar cells and helping me understand the characterization process.

- Janice Hudgings for giving me the opportunity to work in her lab during my sophomore year, convincing me to major in physics, and making me believe, year after year, that it was the right choice.

- My close friends, Rachel Schmidt, Anna Kudla, and Phoebe Tengdin, for making me laugh every day at dinner and giving me thesis related advice despite my ”weird” interests.

- My parents for giving me the opportunity to attend Mount Holyoke and supporting me wholeheartedly in all my pursuits.

- all the Professors in the Mount Holyoke College Physics Department for giving me a wonderful education in physics, giving me the confidence to succeed at Mount Holyoke, and preparing me to face the challenges that await beyond.

Contents

List of Figures

Chapter 1

Introduction and Motivation

This chapter introduces some basic thin film deposition concepts and explains the motivation behind this project. I will begin with a short list of thin film applications, all of which could benefit greatly from the advancement of thin film deposition processes. I will then briefly describe the process of thermal evaporation and the improvements our evaporator makes over existing evaporators. Next, I will describe the process of sputter deposition and the difficulties associated with organic semiconductor device fabrication. Last, I will introduce our novel sputtering system and explain how it attempts to eliminate these difficulties.

1.1 Introduction to evaporation

Thin films, or layers of material ranging from less than a nanometer to several microns in thickness, are becoming increasingly important in today's electronic semiconductor industry.

Organic light-emitting diodes (OLEDs), in which the electroluminescent layer is an organic thin film, provide many advantages for the development of flat panel displays (FPDs) because of their high luminescence, high efficiency, wide color range, easy fabrication processes, and flexibility[8]. In particular, active-matrix organic light-emitting diodes (AMOLEDs), in which the term 'active-matrix' refers to the pixel-addressing technology, are components in many mobile phone and digital camera displays. Moreover, amorphous silicon (a-Si) thin film transistors (TFTs) are proving advantageous in the production of Inverted Top Emission OLED (ITOLED) FPD backplanes because of their simple structure, cheap production processes, and uniform transistor characteristics [10]. Finally, nanostructured donor/acceptor photovoltaics utilizing organic thin films for light absorption and charge transport offer processing advantages that will enable high-throughput, large-area production. If these technologies can meet current manufacturing quotas, sunlight will soon become the cheapest, cleanest, and most abundant source of energy on the planet[11].

In order to study and improve these technologies, researchers need to be able to grow thin films in laboratories. A common thin film deposition method is thermal evaporation. A thermal evaporator consists of a heating mechanism in which source material is contained, a device which suspends substrates above the source material, and a chamber which encloses these components in a high vacuum environment. The source material is heated until it evaporates so that individual particles can rise through the chamber to coat the suspended substrates. The high vacuum environment (typically 10^{-5} to 10^{-8} torr) ensures that the chamber is clear of foreign particles, which allows the evaporated source material to travel straight to the substrates without any collisions, ensures the purity of the deposited layer, and prevents combustion.

Common thermal evaporators, such as those developed by Angstrom Engineering and MBRAUN, tend to be very large, expensive to build and maintain, difficult to clean, and time consuming to use. While these devices are currently being used effectively in premier research laboratories, addressing these drawbacks would provide research opportunities to individuals with less time and

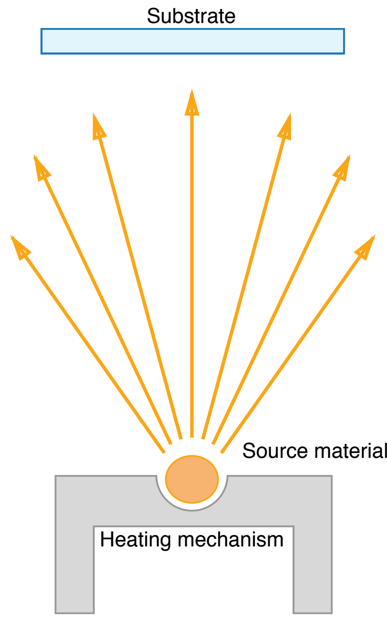

Figure 1-1: Cross-sectional view of standard thermal evaporator set-up.

fewer resources, such as students working at undergraduate universities and liberal arts colleges. Not only will this increase the number of people working in the field, but it will also speed up laboratory processes, resulting in faster progress toward semiconductor development goals.

For this purpose, we have designed and constructed a state-of-the-art thermal evaporator which is inexpensive, simple and quick to operate, and easy to maintain. Its compact size significantly reduces construction costs and pump-down times.

Existing designs situate the evaporator inside the glove box, a sealed glass enclosure accessed by attached butyl gloves which provides an inert nitrogen environment for the fabrication and storage of thin-film devices. Our evaporator is mounted instead beneath the glove box floor with top-loading substrate access from inside the glove box. A retractable base plate elevator system enables access to the chamber from outside the glove box through the chamber floor. These improvements maximize space inside the glove box and accessibility of the evaporator chamber.

An internal metal sleeve which protects the chamber walls from excess source material condensed during evaporation is also included in our design. The sleeve may be removed through the bottom portal, ensuring ease of maintenance.

Our vacuum system consists of a turbomolecular pump connected directly to the chamber as well as external backing and roughing pumps. Yet another advantage of our design is that the backing and roughing pumps are located outside the lab in another room, saving space inside the lab and improving the working environment.

Drawbacks of thermal evaporation include unstable deposition rate control, poor step coverage, and high temperatures of operation. Above all, while the process is well suited for depositing films made of pure metals and organic compounds, alloys and inorganic compounds pose difficulties because of variation in vapor composition throughout deposition. OLEDs and organic photovoltaics require electrodes made of high-quality transparent conducting oxides (TCOs)[8] such as indium tin oxide (ITO) or indium zinc oxide (IZO) [6]. In order to grow these types of layers, sputter deposition is required.

1.2 Introduction to sputter deposition

Drawbacks of thermal evaporation include unstable rate control, poor step coverage and complications associated with deposition of alloys and inorganic compounds [12]. Sputter deposition, on the other hand, can be used to deposit multi-element materials and possesses advantages such as high step coverage, high film adherence and uniformity, good adhesion and high deposition rates [13].

In a typical sputtering device, a neutral gas plasma is generated inside a vacuum chamber by an applied electric field. The energetic ions in the plasma bombard a solid target material, causing atoms to be ejected from the material (or 'sputtered'). These atoms may then condense on a nearby substrate as a thin film. Secondary electrons emitted from the target as a result of ion bombardment play an important role in sustaining the plasma [14]. Chemical reactions at the target surface can be avoided if an inert gas is used as the sputtering medium. Argon is often chosen for this purpose because of its abundance, large size, and low ionization potential [15].

This basic sputtering process has been used successfully for many years, despite limitations such as low deposition rates, low ionization efficiencies in the plasma, and high substrate heating effects. The introduction of the 'conventional' or 'planar' magnetron sputtering system in the early 1970s was an important step toward overcoming these limitations. In this system, permanent magnets situated underneath the target material create a magnetic field parallel to the target surface. In the presence of this field, charged particles in the plasma are subject to the Lorentz force, which is proportional to the component of the particle's velocity perpendicular to the magnetic field. This force causes the charged particles to travel in spiral patterns in the vicinity of the target, increasing the probability of electron-atom collisions near the target surface. This leads to increased ion bombardment of the target, resulting in higher sputtering rates and, therefore, higher deposition rates at the substrate. This increased ionization also allows the sputtering chamber to be held at lower operating pressures (typically 7.5×10^{-4} torr, compared to 7.5×10^{-3} torr) and lower operation voltages (typically -500V, compared to -2 to -3 kV) than is possible in the basic sputtering mode [14].

Sputter deposition systems today possess the same drawbacks as evaporators: complicated and time-consuming operation procedures, high cost of construction, and laborious maintenance procedures. Recently, the process

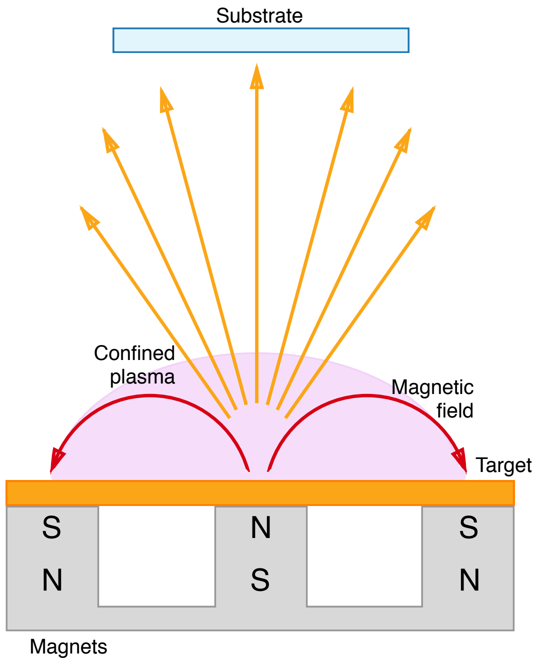

Figure 1-2: Cross-sectional view of the planar magnetron configuration.

has developed a new problem. The fabrication of many semiconductor devices involves deposition by sputtering onto a substrate previously coated with an organic thin film. However, energetic particles in the sputtering plasma have been shown to cause critical damage to underlying organic layers on substrates during sputter deposition. The kinetic energy of charged particles in the sputtering plasma is sufficiently high to break most of the carbon-based bonds in the organic materials. The destruction of these bonds creates micro-current paths through the organic layers which degrade device performance [16]. The magnetic field in the planar magnetron configuration protects substrates to some extent, typically confining the densest region of plasma to within 60 mm of the target [14]. However, it is difficult to perfectly match the strength of the inner magnet with the outer magnets shown in Figure 1-2. When these magnets are mismatched, charged particles can escape the plasma along stray field lines generated by the stronger of the magnets, so that a significant amount of substrate damage still occurs [13]. This damage must be reduced in order

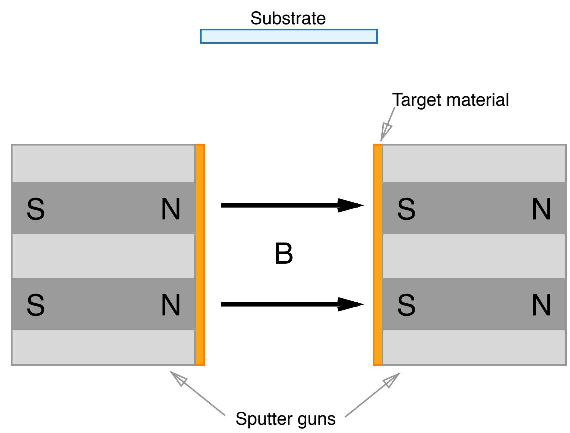

Figure 1-3: Cross-sectional diagram of the facing target sputtering configuration.

to fabricate high quality organic semiconductor devices.

For this purpose we have designed a novel low-damage sputtering system, which shares all the features of our evaporator listed in Section 1.1. In order to ensure the most effective design, we conducted a literature search for low-damage sputtering techniques. These are reviewed in detail in Section 4.1.

Previous studies indicate that the facing target sputtering configuration is the most consistently effective and well understood of the known low-damage sputtering methods. In this configuration, two magnetron sputter guns are aligned vertically parallel, with their targets facing one another. The substrate is positioned perpendicular to the target plane, as shown in Figure 1-3. The facing target method has been shown to confine the sputtering plasma below the substrates better than the standard planar sputtering configuration. Furthermore, it would be possible to arrange sputter guns ordered from commercial vendors in this configuration, whereas many of the other methods require elaborate custom designs. Consequently, our sputter system design takes advantage of the facing target method.

We also wanted to utilize sector-shaped shields proposed by Lei et. al., which cover the outer portions of the targets closest to the substrates. These shields are believed to block high energy secondary electrons emitted from the edges of the targets that would otherwise have escaped the confining magnetic field between the targets and struck the substrates. These were not difficult to add to our design, so we made provisions for them as well.

In addition to these low-damage design features, we have added our own novel feature that we believe will decrease energetic particle bombardment of the substrates. In all documented instances of the facing target sputtering configuration, there is a space between the substrates and the magnets generating the confining magnetic field. This creates a region near the substrate where the magnetic field is weaker and the field lines bend toward the substrates, as shown in Figure 1-4a. Any charged particles traveling along these field lines will be unaffected by the Lorentz force, and will have a clear path to the substrates.

We predict that adding additional high strength permanent magnets between the targets and the substrates as shown in Figure 1-4b, generating a magnetic field parallel to the field between the targets, will help to contain these stray particles and further protect the substrates. These extra magnets will effectively extend the magnetic field created by the sputter guns outside of the plasma generation region, so that even the particles that escape the region of dense plasma between the targets will be confined in some space. These magnets might even make the target shields suggested by Lei et. al. unnecessary.

The purpose of this project is, first, to improve thin film deposition methods in terms of cost and ease-of-use, and second, to facilitate the fabrication and investigation of high quality electronic devices with cutting-edge device architecture. I will provide all background information needed to understand the project in Chapter 2. Chapter 3 will describe our evaporator design in detail and discuss its improvements over existing designs. Chapter 4 will de-

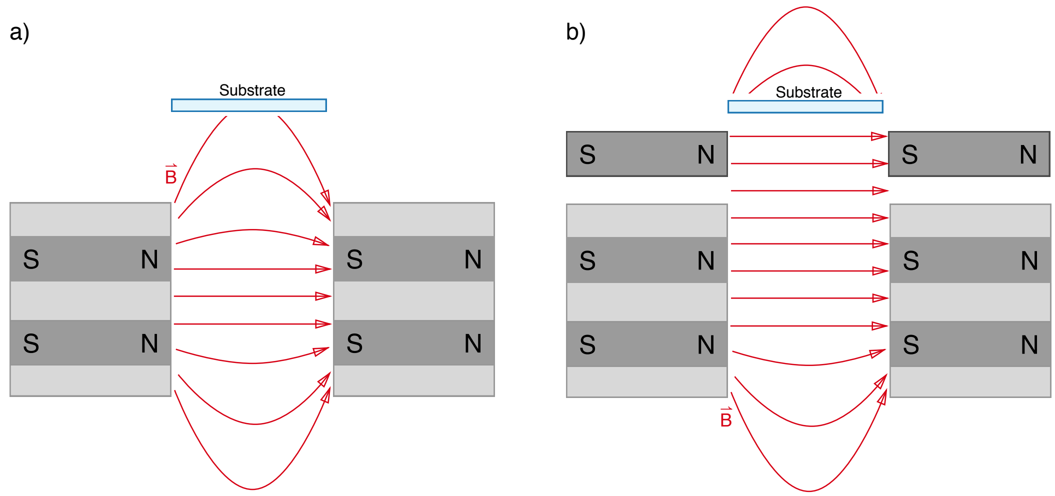

Figure 1-4: a) The magnetic field generated by the sputter guns grows weak and the field lines bend toward the substrates at the top edges of the targets. Charged particles can escape the dense plasma region between the targets and travel along these lines to strike the substrates. b) We predict that adding additional magnets in this region will strengthen the magnetic field and straighten the field lines between the targets and the substrate, further protecting the substrate from energetic particles.

scribe our sputtering system in detail and discuss its potential for low-damage thin film deposition. Finally, in Chapter 5, I will summarize the project and its implications for future thin film device development.

Chapter 2

Background

This chapter provides all background information necessary to understand thin film deposition processes as they pertain to our project. I will begin with an elementary discussion of vacuum technology, including gas properties, materials used in vacuum systems, and vacuum flanges and fittings. I will then provide a detailed description of the evaporation process, focusing on source heating methods, deposition patterns, and complications associated with the deposition of alloys and inorganic compounds. Finally, I will provide a detailed description of the sputtering process, including plasma generation, sputter sources, and reactive sputtering processes.

2.1 Vacuum Technology

Both evaporation and sputter deposition are performed under some degree of vacuum. Consequently, it is important to understand some basic aspects of vacuum technology in order to understand these processes.

An important characteristic of a contained gas at any pressure is the mean free path of a given particle. This is defined as the mean length of path a particle travels before colliding with another particle. It is given by:

$$\lambda(m) = \frac{1}{\sqrt{2}\pi d_0^2 n} \tag{2.1}$$

where d_0 is the molecular diameter in meters and n is the gas density in molecules per m^3. The mean free path is gas density dependent, and pressure dependent if the temperature is held constant. Using the ideal gas law, $P = nkT$, where P is pressure, k is the Boltzmann constant, and T is the temperature in kelvin, to substitute for n, Equation 2.1 can be written as:

$$\lambda = \frac{kT}{\sqrt{2}\pi d_0^2 P} \tag{2.2}$$

Knowing the mean free path of source molecules during thin film deposition can provide information about the deposition rate and the conformity of the film. A short mean free path results in a low deposition rate, since the source molecules must undergo many collisions before reaching the substrate, as well as conformal step coverage, because collisions with gas molecules make the source molecules more likely to impinge on the substrate at oblique angles.

A useful property for examining the pumping process is gas throughput, which is defined as the volume of gas at a known pressure that passes a plane in a known time. At constant temperature, the gas throughput describes mass flow. Gas throughput can help us understand pumping speed, which is the volumetric rate at which gas is transported across a plane. It is equal to the gas throughput divided by pressure at a plane of a pressure gauge.

An important consideration when designing a vacuum system is the type of material used for each component. All gas could be pumped from a vacuum chamber in an extremely short time if it were located within the volume of the chamber. In reality however, gases and vapors on the surface and within pores in interior chamber walls desorb slowly in a process known as outgassing. These vapors add to the gas that must be removed from the chamber and considerably retard the pump-down process. While baking can minimize outgassing to some extent, vacuum chambers with large internal surfaces cannot be baked and so must be fabricated from appropriate materials, as will be described below.

As well as minimizing outgassing, the vacuum chamber must be able to withstand a pressure load from atmosphere of at least 10,335 kg/m^2. The most common metals used in vacuum chambers are aluminum and stainless steel. Aluminum is easy to fabricate but is difficult to join to other metals. For this reason, stainless steel is usually preferred for modern vacuum chambers.

The types of flanges used to attach demountable joints must also be considered when designing a vaccuum system. The most common vacuum seals are made with either elastomer or copper. Elastomeric compounds store elastic energy, conform to fit surface irregularities, resist chemicals and can be repeatedly used. However, they cannot withstand high baking temperatures or plasma bombardment. Elastomer seals are made by deforming an elastomeric ring called an O-ring between two flat surfaces or confining it in a groove. The most commonly used elastomeric seal is the ISO-KF (kleinflansch), which uses a centering ring to position a standard size O-ring between two flanges, and a clamp to compress the O-ring. O-rings can also be mounted on flat surfaces using a dovetail or half-dovetail groove. The trapezoidal cross sections of these grooves, shown in Figure 2-1, hold the O-ring in place.

Elastomers are inadequate for many applications due to high outgassing rates and their inability to withstand high temperatures. Therefore, it is often necessary to use metal gaskets in demountable joints. Though metal gaskets have much lower outgassing rates than elastomers and can withstand high temperature baking, they don't return to their original shape after the compressing flange surfaces are removed. This means that the gasket must be

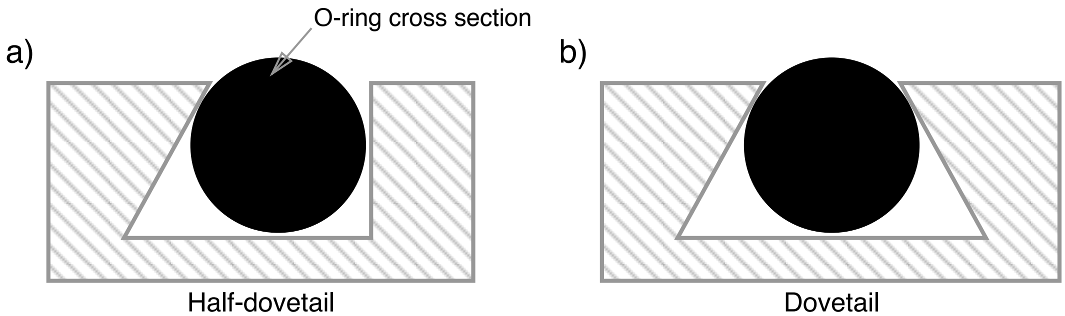

Figure 2-1: When an o-ring groove is cut into a flat surface, it is necessary to make sure the o-ring won't pop out. This can be done with a) a dovetail groove or b) a half dovetail groove.

replaced every time a flange is opened, so metal seals are best used on parts that do not have to be frequently exposed to atmosphere.

The most commonly used metal seal is the ConFlat (CF) seal, which uses a copper ring gasket. It consists of two symmetrical flanges, each containing a hardened knife edge. The flanges are tightened until they touch and capture a section of the copper gasket between the knife edge and the outer surface of the flange. This forces the copper to flow into surface irregularities with a high pressure.

Motion can be translated from outside the chamber to parts inside the chamber using rotary and linear feedthroughs. These all use some form of an elastomer or metal seal in combination with a moveable metal bellows. A detailed account of vacuum technology is given in John F. O'Hanlon's *A User's Guide to Vacuum Technology* [17], and in Chapters 2 and 3 of Donald L. Smith's *Thin-Film Deposition* : *Principles and Practice* [18].

2.2 Evaporation

Now that we have discussed some aspects of vacuum technology, we are in a better position to understand the physical vapor deposition processes of evap-

Figure 2-2: The dimpled sheet-metal "boat" is the most commonly used resistive evaporation source [1].

oration and sputtering. We will begin with evaporation.

An evaporator consists of a heating mechanism in which source material is contained, a device which suspends substrates above the source material, and a chamber which encloses these components in a high vacuum environment. The source material is heated until it evaporates, so that individual particles can rise through the chamber to coat the suspended substrates. The high vacuum environment (typically 10^{-5} to 10^{-8} torr) ensures that the chamber is clear of foreign particles, which allows the evaporated source material to travel straight to the substrates without any collisions, as well as ensuring the purity of the deposited layer and preventing combustion.

Standard system components include a stainless steel chamber, high vacuum pumping capacity, pressure gauges, evaporation sources and power supply, and substrate holder.

The most common evaporation sources rely on resistive heating to evaporate source material. The simplest of these is the dimpled sheet-metal boat shown in Figure 2-2. In order to heat the source material, a power supply passes a current on the order of 100 amps through the boat. The boats are resistive enough that, as current flows through them, a significant amount of power is dissipated as heat, which is then transferred to the source material. Boats are low-capacity sources and are usually used only in lab experiments. Ceramic crucibles provide better temperature uniformity and control than boats and are more suited to large-scale applications. Inductively heated sources and electron beam sources also have advantages for large-scale applications.

Since evaporation takes place at such low pressure, the mean free path for evaporated source atoms is very large (500 to 10^5 cm) relative to the substrate-to-source distance. This means that the atoms undergo collisionless line-of-sight transport to the substrate, resulting in a film deposition pattern known as the "cosine distribution." For evaporation from a small area onto a parallel plane receiver, the deposition rate is proportional to $\cos^2\theta/r^2$ and the thickness distribution is given by:

$$\frac{t}{t_0} = \frac{1}{(1+(\frac{x}{h})^2)^2} \tag{2.3}$$

where t_0 is the film thickness vertically above the source at a distance h, and t is the film thickness a horizontal distance x from the vertical line. These variables are diagrammed in Figure 2-3. According to Equation 2.3, the film thickness will decrease by about 10% for $x = \frac{h}{4}$. This nonuniform deposition is one of the central drawbacks of evaporation. Solutions to this problem include substrate motion and strategically shaped sources, but these solutions are often inconvenient or expensive to implement.

For a single element source material, the rate of evaporation is determined by the vapor pressure, which is in turn determined by the source temperature. However, for alloys and inorganic compounds, evaporation rates are more complicated. In the case of alloys, the two components have different vapor pressures, and hence different evaporation rates. This means that the composition of the deposited material varies constantly throughout deposition. In the case of compounds, evaporation can occur with or without dissociation of the source molecules into fragments. Most organic materials do not disso-

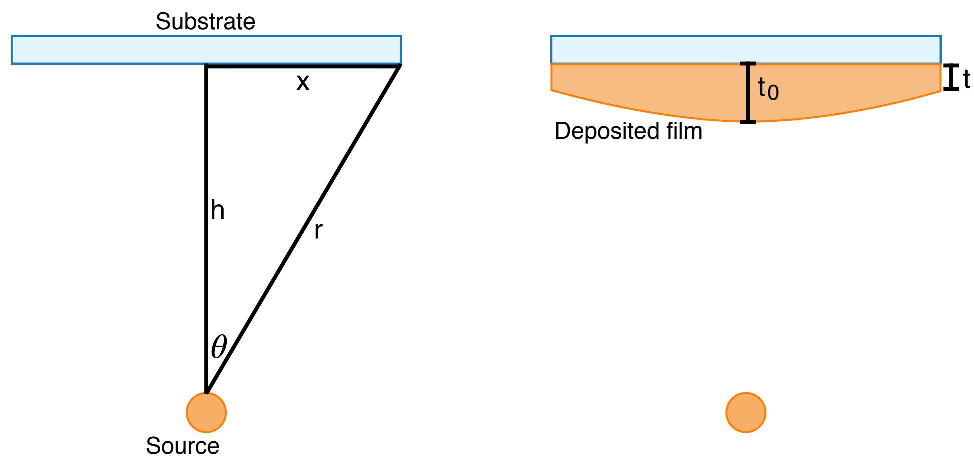

Figure 2-3: Schematic diagram of variables in Equation 2.3, the cosine distribution law.

ciate, making deposition by evaporation an excellent choice for these types of films. However, only a few inorganic compounds evaporate without dissociating. Once the source molecules dissociate, a great number of factors must be controlled in order to achieve stoichiometric film composition.

This can be done by reactive evaporation, in which a reactive gas is introduced into the chamber during evaporation. However, these methods are extremely complicated and often expensive. A simpler solution is sputter deposition. A detailed account of the evaporation process is given in Chapter 2 of John L. Vossen and Werner Kern's *Thin Film Processes*, *Volume* 2 [13], and in Chapter 4 of Donald L. Smith's *Thin-Film Deposition* : *Principles and Practice* [18].

2.3 Sputter Deposition

In addition to its ability to grow multi-element materials, sputter deposition possesses several advantages over evaporation such as high step coverage, high film adherence and uniformity, good adhesion and high deposition rates. However, sputter deposition is inadequate for growing organic films because bombardment by energetic particles breaks chemical bonds, destroying organic structure.

In a typical sputtering device, a neutral gas plasma is generated inside a vacuum chamber by an applied electric field. The energetic ions in the plasma bombard a solid target material, causing atoms to be ejected from the material (or 'sputtered'). These atoms may then condense on a nearby substrate as a thin film. In order to avoid chemical reactions at the target surface, an inert gas is required as the sputtering medium. Argon is often chosen for this purpose because of its abundance, large size, and low ionization potential. As will be seen in Section 2.3.4, chemical reactions at the target surface are sometimes desirable. In these cases a reactive gas, such as oxygen, is used as the working gas. Sputter deposition is usually performed around $5 * 10^{-3}$ torr because very low pressures will inhibit plasma generation and maintenance. However, the system must be brought down to about 10^{-6} torr prior to plasma generation in order to clear the chamber of unwanted molecules and allow greater user control over the materials present in the chamber.

Standard parts include a stainless steel chamber, pumping capacity down to 10^{-6} torr or lower, pressure gauges, means to raise chamber pressure to $\approx 5 * 10^{-3}$ torr for operation (mass flow controller and variable gate valve), sputter sources and power supply, and substrate holder.

2.3.1 Plasma characteristics

In order to understand the sputter deposition process it is first important to understand certain plasma characteristics. A plasma is a partially ionized gas consisting of nearly equal concentrations of electrons and ions, rendering it effectively neutral. It is considered the fourth state in a progression of increasingly energetic states of matter (the others being solid, liquid, and gas).

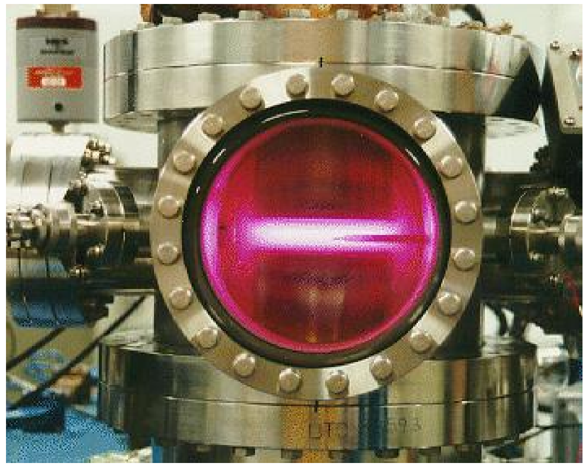

Figure 2-4: Photograph of argon plasma inside a vacuum chamber [2].

Particles in the plasma often collide, resulting in excitation and relaxation of atoms and ions. This results in photon emission, which accounts for the plasma's glowing quality. The color of emission is determined by the type of gas molecules in the plasma. Sputter deposition utilizes a glow-discharge plasma, which is characterized by low pressure and diffusivity. Ionization fraction in a glow-discharge is very low, ranging from 10^{-5} for 10^{-1}. Electron energy ranges from 1 to 10 eV, while ion energy ranges from .02 to .1 eV. Ionization energy, or the energy it takes to ionize an atom, ranges from .1 to 20 eV.

Processing plasmas must be driven by external power supplies whose frequencies may vary from DC to 10 GHz and powered up to 30 kW. Several techniques are used to generate processing plasmas. However, the most common method involves applying a high voltage across a set of metal electrodes. This creates an electric field between the electrodes with magnitude V/d, where d is the distance between the electrodes. This method relies on ionization of background gas by fast primary electrons, or electrons emitted by the cathode. In a DC powered system, the gas conditions are very important for effective generation. If gas density is too low, the electrons are likely to reach the anode without colliding with a gas atom. If the density is too high, the electrons are likely to collide with atoms before gaining sufficient energy to ionize them. Appropriate gas pressures for effective generation generally range from .1 to 1000 mtorr. When an electron collides with an atom with enough energy to ionize it, an extra electron is created as well as an ion. The ion will be accelerated towards the cathode and the two electrons will be accelerated towards the anode. Under the right conditions, additional ionization occurs. High energy collision of ions with the cathode cause emission of electrons called secondary electrons, which contribute to the ionization process as well. With the right gas density and applied power, electrical breakdown rapidly occurs.

Several plasma features are important for thin film deposition. The first is the plasma potential. As a plasma is generated, the electrons repel each other and the ions repel each other. This repulsion causes the charged particles to spread out until they reach a confining obstacle, such as the walls of the sputtering chamber. Because of their small mass, the electrons travel more quickly than the ions, causing the chamber walls to build up negative charge, and a potential difference to develop between the plasma and the walls. Since the chamber walls are grounded, this means the plasma's potential is positive. The potential at which the loss rate of electrons into the chamber walls is equal to the loss rate of ions is referred to as the plasma potential. Because of this phenomenon, the plasma will always be more positive than its most positive containing surface by a minimum of several volts. Though the potential drops at the extreme edges, the plasma potential is constant throughout the plasma bulk.

Similarly, an electrically floating surface in the sputtering chamber will rapidly charge negatively because of the high electron diffusion rate. This is called a floating potential. This phenomenon has been used to create ion beams, since the ions in the plasma are accelerated towards this negative surface.

The positive nature of the plasma potential gives rise to another plasma characteristic called the sheath, which is a dark space adjacent to all confining surfaces. The large voltage drop at the edges of the plasma results in a region of low electron density near the chamber walls, since the electrons are repelled by the negatively charged walls. The low electron density results in low levels of excitation in gas molecules, and therefore low photon emission rates, causing the area to appear dark. A detailed account of glow-discharge plasma physics is given in Chapter 1 of John L. Vossen and Werner Kern's *Thin Film Processes*, *Volume* 2 [13], and in Chapter 9 of Donald L. Smith's *Thin-Film Deposition* : *Principles and Practice* [18].

2.3.2 Non-magnetron sputter sources

Next we must consider how sputter systems utilize the glow-discharge for film deposition. The simplest system configuration is the DC diode, in which the substrates and target face each other, acting as two electrodes. These are connected by an external high-voltage power supply. The target, which acts as the cathode, is typically disk-shaped with a diameter ranging from 5 to 10 cm. The target must be thermally bonded to a water-cooled backing plate to dissipate heat created by bombardment and prevent outgassing or melting of the target material. A ground shield is used to suppress undesirable sputtering of the source support body. Plasma is generated using the method described in the previous section with operating pressures generally between .1 and 1000 mtorr.

Weaknesses of this configuration include low deposition rates and inefficient use of secondary electrons. Bombardment of the growing film by energetic electrons and ions must also be considered. This is often desirable because certain high quality film characteristics can be achieved by substrate bombardment during film growth. However, in the case of delicate substrates, bombardment can cause significant damage.

Another drawback of the DC diode system is its inadequacy for depositing insulating films. Secondary electron emission results from energetic ion bombardment of the target, regardless of its material. However, when an insulating material is used, electrons are unable to flow from ground to replace emitted secondary electrons, resulting in a positive charge on the target. This causes the target to repel bombarding ions, stalling the sputtering process.

This problem can be corrected by applying an alternating current to the electrodes, so that the polarity of the target reverses, attracting electrons from the discharge to eliminate the surface charge. The AC frequency must be high enough to neutralize charge build-up but low enough to maintain the flux of ions impinging on the target. This is achieved by the RF diode configuration. This set-up is usually the same as the DC diode: two electrodes, one of which is powered and one of which ties to ground. Alternatively, the two electrodes can be connected to the same power supply or each connected to a separate power supply. Most systems operate at 13.56 MHz because of government communication regulations.

Aside from allowing the use of insulating targets, this configuration also increases the level of ionization in the plasma because the oscillating applied field is more efficient at increasing net electron energy. Additionally, the plasma sheath will oscillate in this configuration. The electrons can ride this oscillation and gain extra energy. However, above 1 to 2 keV, the sputtering process becomes less efficient per watt, and deposition rates will no longer rise linearly with power. Secondary electron energy will also continue to increase with power, which can cause severe damage to substrates. Because of this, the RF diode is best operated below 5 kW.

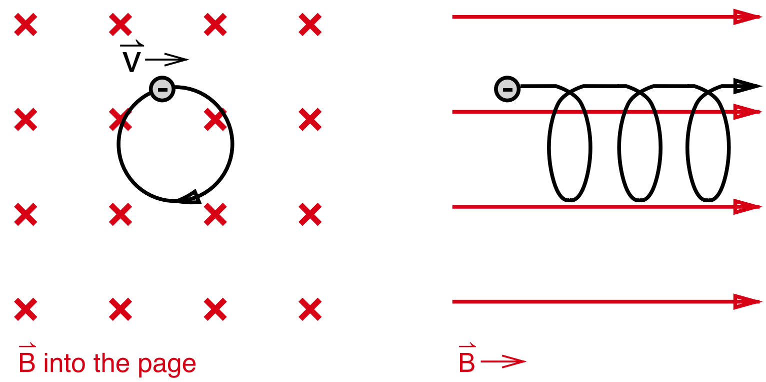

Figure 2-5: In a constant magnetic field, a charged particle will experience a force proportional to the component of its velocity perpendicular to the magnetic field, causing it to travel in a circle. If a component of the particle's velocity is parallel to the magnetic field, the particle will continue to travel in that direction.

2.3.3 Magnetron sputter sources

The DC and RF diode are only moderately effective sputtering configurations. Much better deposition conditions can be achieved using magnetron sputter sources. In order to understand how these work, it is first important to understand plasma behavior in magnetic fields.

Moving charges in the plasma are subject to the Lorentz force, given by:

$$F = q(\vec{v} \times \vec{B}) \tag{2.4}$$

where q is the charge of the particle, v is the particle's velocity, and B is the magnetic field. In a constant magnetic field, this means that a charged particle will feel a centripetal force proportional to the component of its velocity perpendicular to the magnetic field. This causes the particle to travel in a circle, as shown in Figure 2-5. The radius of the circle is given by:

$$r = \frac{mv_\perp}{qB} \tag{2.5}$$

where m is the mass of the particle and and $v_\perp$ is the component of the velocity perpendicular to the magnetic field. The Lorentz force will have no effect on a particle traveling parallel to the magnetic field. If a component of the particle's velocity is parallel to the magnetic field, it will travel in a looping pattern, also shown in Figure 2-5. Equation 2.5 can be given in terms of the particle's kinetic energy as well:

$$r = \frac{\sqrt{2m(KE)}}{qB} \tag{2.6}$$

where KE is the kinetic energy of the particle. This equation is more useful for calculating Lorentz radii in plasmas. For example, consider an electron and an argon atom, both with energies of 50 eV, in a magnetic field with magnitude 500 gauss. The electron's orbital radius will be equal to .34 mm, while the ion's will be 47 cm.

If an electric field is present as well, charged particles will tend to drift in the direction given by the cross product of the electric field and the magnetic field. This is because, at a certain velocity of the particle, the electric and magnetic forces on the particle add to zero, so that the particle's motion is unaffected by either field. This is known as the E×B drift. The velocity of the particle at which this effect occurs is given by:

$$v_{E\times B} = \frac{E}{B} \tag{2.7}$$

where E is the magnitude of the electric field and B is the magnitude of the magnetic field. If a plasma is contained in a region with a constant magnetic field and perpendicular constant electric field, as shown in Figure 2-6, the charged particles will tend to drift towards one side of the plasma and be lost. The magnitude of the E×B drift velocity is greatest when the electric and magnetic fields are perpendicular, and zero when they are parallel.

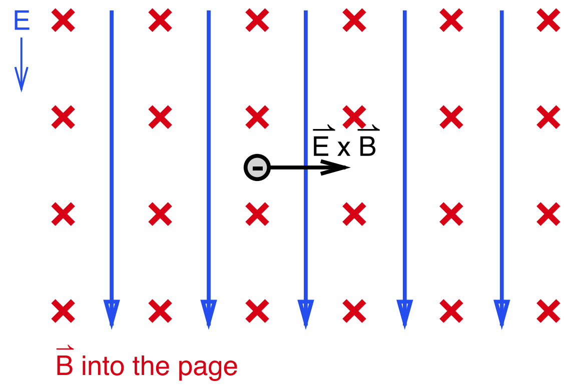

Figure 2-6: A charged particle in a region containing perpendicular electric and magnetic fields will tend to drift in the direction given by the cross product of the electric field and the magnetic field. This is known as the E×B drift.

The magnetron sputter source takes advantage of the behavior of plasmas in magnetic fields to create a much more effective deposition environment than the non-magnetron sources. A typical planar magnetron sputter source is similar to the non-magnetron source described in section 2.3.2 above, but includes a magnetic field of 50 to 500 gauss parallel to the target surface, generated by permanent magnets just underneath the target material. This sputter source doubles as a source of sputtering gas, which diffuses through a circular opening around the target surface as shown in Figure 2-7. This structure is also referred to as a sputter gun.

The magnetic field is usually generated by an inner and an outer ring magnet. The inner magnet's north side is oriented towards the target surface while the outer magnet's south side is oriented towards the target surface, generating the magnetic field shown in Figure 2-8. Not only does the Lorentz force due to this field cause electrons to spiral near the target surface, the E×B drift path also forms a closed loop around the perimeter of the target, preventing electrons from being lost from the plasma.

The spiraling effect caused by the magnetic field increases the electron path length significantly, making collisions with the target more likely and in-

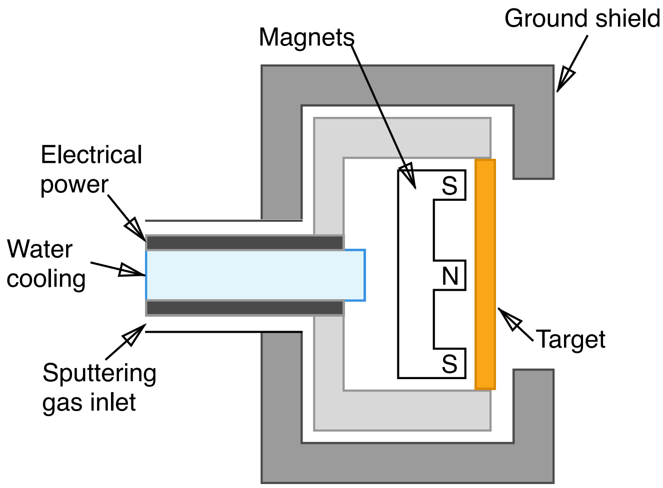

Figure 2-7: Cross-sectional diagram of a standard magnetron sputtering source.

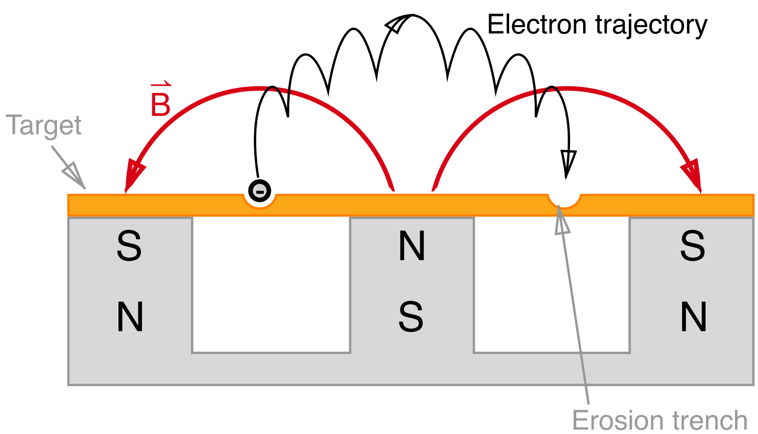

Figure 2-8: Magnetic field and electron trajectory created by a standard planar magnetron sputtering source.

creasing the net density of electrons and ions in the plasma. The magnetic field doesn't directly affect ion motion because the ions' Lorentz radii will often exceed the ion mean free path, if not the substrate-to-target distance. However, electrostatic attraction causes the ions to move with the electrons, keeping the plasma neutral. This results in a denser, less resistive plasma which means that discharge voltage, or the voltage difference between the electrodes, at constant power is lower than without a magnetic field. With the magnetron, the efficiency of the sputtering process increases so that the system can operate at low pressure (1-3 mtorr) and low voltage (350 V). The low operating pressure means that the deposition rate can increase significantly, since the target material will collide with fewer gas molecules before reaching the substrate. RF and DC power both work well in this configuration.

Though the magnetron sputter source makes the sputter deposition process much more efficient, it does have several drawbacks. The current density at the cathode is peaked where the magnetic field lines are tangent to the surface of the cathode as shown in Figure 2-8, meaning that this is where the most surface bombardment occurs. This means that the target erodes non-uniformly during deposition and only 20 to 30 % of the starting target material is used. Moving the target with respect to the magnets can overcome this problem, but this considerably complicates system set-ups.

Second, though much of the plasma discharge is confined close to the cathode surface by the magnets, ion fluxes at the substrate surface are still typically 5 to 10% of the deposition flux. This is because it is very difficult to perfectly match the strengths of the inner and outer ring magnets in the sputter source. When these are mismatched, the field lines generated by the stronger of the two magnets begin to bend away from the weaker magnet and toward the substrate, as shown in Figure 2-9. A charged particle traveling parallel to one of these lines is unaffected by the Lorentz force, and has a clear

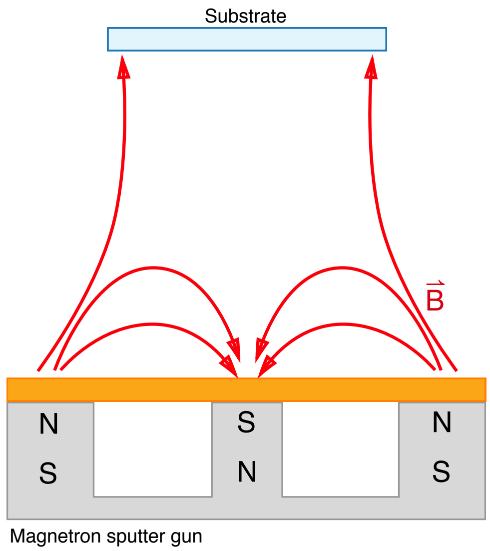

Figure 2-9: Because it is very difficult to perfectly match the strengths of the inner and outer ring magnets in the sputter gun head, field lines of the stronger of the two magnets bend away from the opposing magnet and toward the substrate, allowing some bombardment of the substrate by charged particles.

path to the substrate. For applications requiring minimum bombardment, this means it may be necessary to increase operating pressure and substrate-to-target distance, which results in slower deposition rates and lower quality films. If substrate bombardment is desired, the unbalanced magnetron, in which one magnet is purposefully stronger than the other, is an option.

Typical magnetron sputtering characteristics include cathode current densities up to 20 mA/cm^2, discharge voltages between 250 and 800 V, and minimum operating pressure of 1 mtorr. Substrate-to-target distance ranges from a few centimeters to 20 cm, and deposition rates range from 100-2,000 $\mathring{A}$/min.

2.3.4 Reactive sputtering

Any type of sputter source, DC, RF, or magnetron can be used to fabricate metallic films, and RF can be used to fabricate insulating films. However, though multicomponent targets such as oxides and nitrides are sputtered stoichiometrically from the target, they do not condense stoichiometrically on the substrate. This is because of different sticking coefficients of the the two components.

Consequently, these types of materials must be deposited by reactively sputtering a metal target (RF or DC power) in a mixture of an inert gas (usually argon) and a suitably reactive gas. The amount of reactive gas present in the chamber must be carefully controlled in order to ensure the correct ratio of components in the deposited film. The reactive gas can be introduced into the chamber through the same opening in the target as the inert gas. Using this method, deposition rates comparable to those of pure metals can be achieved and different types of dielectrics can be fabricated by choosing different reactive gas mixtures. A detailed account of the sputter deposition process is given in Chapter 4 of John L. Vossen and Werner Kern's *Thin Film Processes*, *Volume* 2 [13], and in Sections 9.3.3 and 9.3.4 of Donald L. Smith's *Thin-Film Deposition* : *Principles and Practice* [18].

Chapter 3

Evaporator Design

This chapter gives a detailed account of our evaporator design process. I will begin with a brief overview of existing evaporator designs and their drawbacks, then provide a component-by-component description of our design. Next, I will describe the process of fabricating a cutting-edge photovoltaic device using our evaporator. I will end with a discussion and evaluation of our design's success in terms of low cost and usability.

3.1 Overview of existing devices

Existing thermal evaporators, such as those developed by Angstrom Engineering and MBRAUN, tend to be very large, expensive to build and maintain, difficult to clean, and time consuming to use. While these systems are currently being used effectively in premier research laboratories, addressing these disadvantages would provide research opportunities for individuals with less time and fewer resources, such as students working at undergraduate universities and liberal arts colleges. This will speed up laboratory processes, resulting in faster progress toward semiconductor development goals.

First of all, existing evaporators cost over $200k on average to build, and

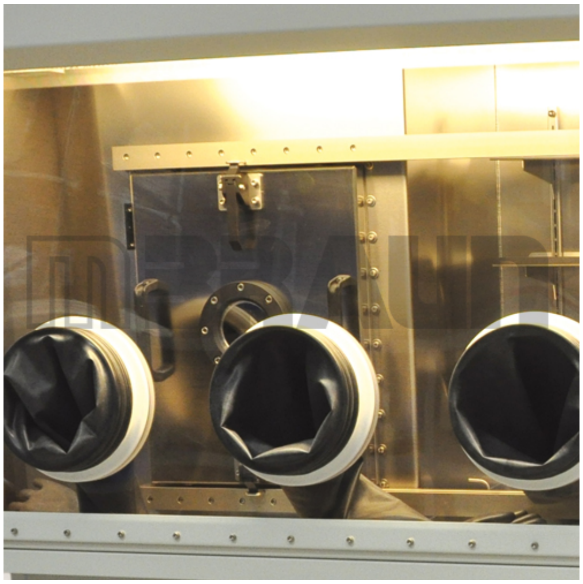

Figure 3-1: Evaporator chamber built by MBRAUN Engineering, situated inside glove box and accessible through a front door [3].

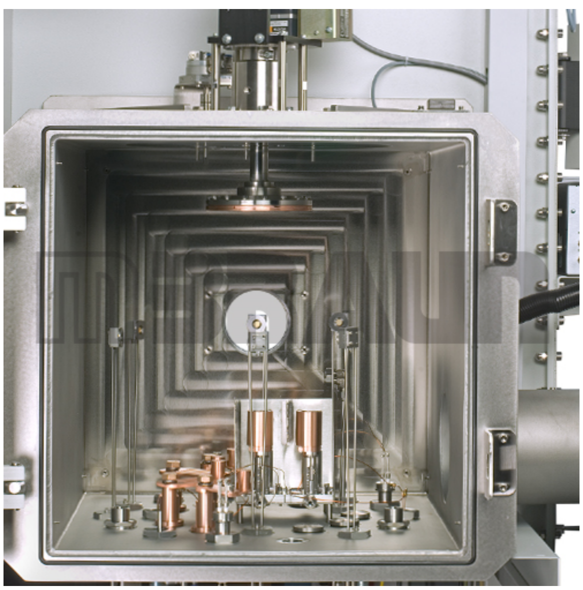

Figure 3-2: Common evaporator chambers tend to be needlessly large, with lots of wasted space inside [3].

parts can be expensive to replace. Some of this expense is due to the large size of the process chambers. Not only do these chambers waste space, but they can also take hours to pump down to operating pressure, which makes for prolonged laboratory fabrication processes.

Second, these chambers are usually located inside the laboratory's glove box, where they occupy a significant amount of space that could be otherwise useful. This also forces laboratory workers to use the cumbersome butyl glove box gloves to manipulate the system. Because these chambers are usually accessible through a front door, laboratory workers must reach inside the chamber to handle delicate interior system components. This can be difficult to do while wearing the restrictive glove box gloves.

Last, these systems tend to be time consuming and difficult to clean. Common deposition chambers are equipped with shielding devices that protect the chamber walls from vaporized material during deposition. These devices are usually composed of many pieces, each of which must be removed from the chamber separately during cleaning. This process can take a team of people as much as an afternoon to complete.

3.2 Novel Design

In order to expand the field of thin film research to a wider group of researchers, we have designed and constructed a state-of-the art thermal evaporator which is inexpensive, simple and quick to operate, and easy to maintain. I will provide a detailed description of each of the design's components, which include torpedo-style vacuum chamber, retractable base plate elevator system, source heating mechanism, substrate holder and mask assembly, substrate rotation mechanism, metal sleeve, shutter, thickness monitor, and vacuum system. CAD models for all system components were created in SolidWorks 2010.

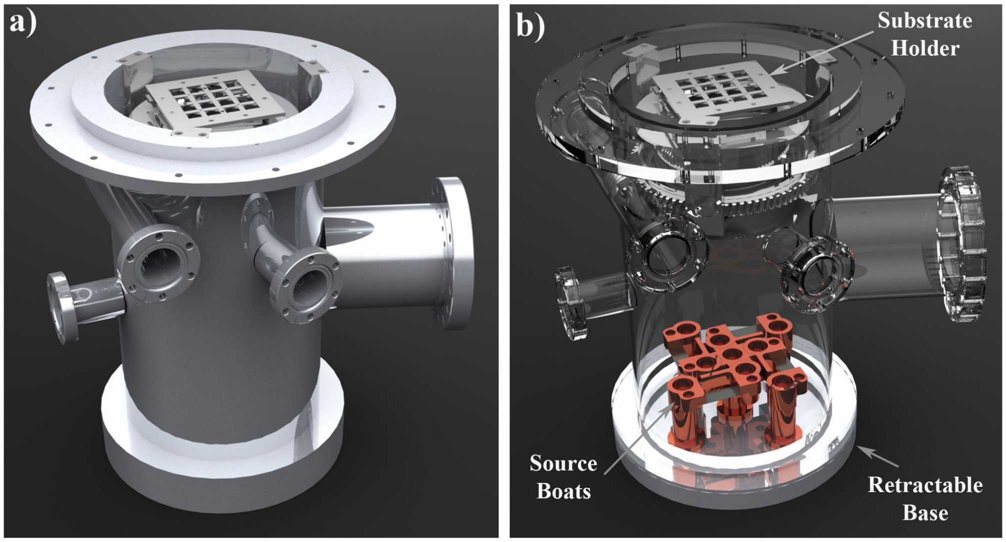

Figure 3-3: a) SolidWorks representation of Torpedo style evaporation chamber b) SolidWorks representation of evaporation chamber with substrate holder, source boats, and base plate shown.

3.2.1 Torpedo chamber design

The evaporator chamber is 8" in diameter and 15.75" tall (including the .97" base plate). Its height was chosen based on a 12" maximum throw distance between the evaporation sources and substrates. This distance can be modified, as will be seen in section 3.2.4, so that it effectively ranges from 9.95" to 11.73". The chamber's small size allows for pump-down times under 3 minutes in nitrogen, and 30 minutes from ambient atmosphere.

In contrast to the existing evaporator designs in which the chamber is situated inside the glove box, our chamber is mounted beneath the glove box floor as shown in Figure 3-4. The top flange of the chamber is 9 inches in diameter (OD) and is sealed to the glove box floor with an o-ring in a half dovetail groove.

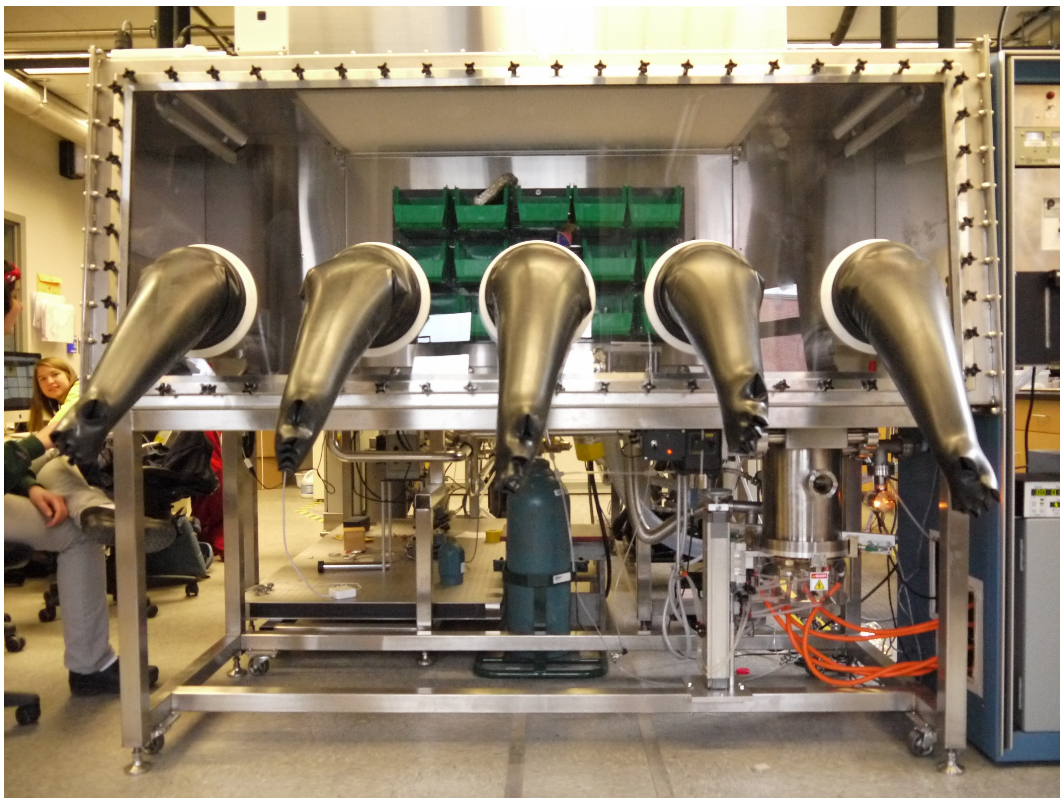

Figure 3-4: The evaporator chamber is mounted underneath the glove box instead of inside it, saving space inside the glove box and ensuring accessibility of the chamber.

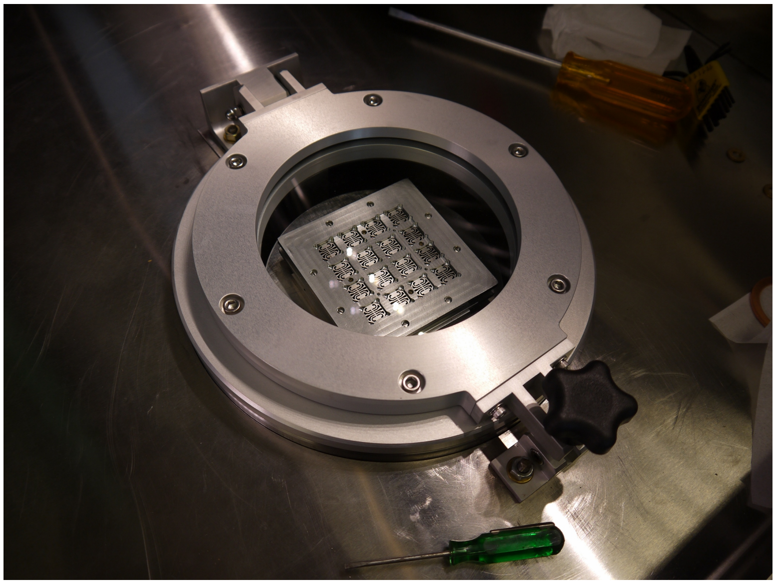

Figure 3-5: The evaporator chamber is accessible from inside the glove box through a port in the glove box floor

The top opening of the chamber is accessible from inside the glove box through a hinged port with viewing window. Situating the chamber this way maximizes space inside the glove box and allows laboratory workers to access components attached to flanges on the outside of the chamber without using the glove box gloves.

3.2.2 Retractable base plate elevator system

While the top opening of the chamber is accessible from inside the glove box, a retractable base plate elevator system enables access to the chamber from outside the glove box through the chamber floor. The 9.97" diameter base plate is attached by a 6.42" arm to a metal post near the chamber. A screw gear lifts the arm along a groove in the post and specially designed clamps fasten the base plate to the bottom lip of the chamber during pump-down. A 9" o-ring in a half dovetail groove ensures a high vacuum seal between the base plate and the chamber.

Figure 3-6: A retractable base plate elevator system allows access to the evaporation chamber from outside the glove box.

The clamps can be removed when bringing the chamber up to atmospheric pressure so that the base plate falls open. A spring extending vertically near the bottom of the post catches the base plate when it falls. A hinge on the extending arm allows the base plate to rotate outward from underneath the chamber, providing access to the heating sources. This is an improvement over designs featuring access through a front door in which the inside components are often difficult to reach.

3.2.3 Source heating mechanism

The source heating mechanism is located on the chamber's base plate so that it can be easily accessed from outside the chamber. We chose resistive evaporation using boats rather than crucibles because it is a cheaper method and

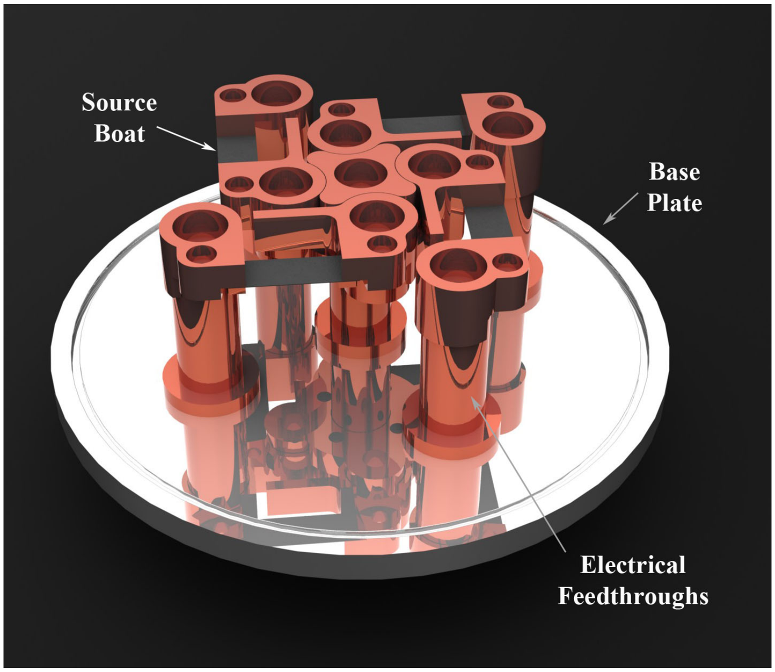

Figure 3-7: SolidWorks representation of source heating mechanism, with source boats, electrical feedthroughs, and base plate shown.

more suited to small scale applications. Our system is capable of holding four different types of source material at once, making it possible to deposit multiple layers of a device without bringing the chamber up to atmospheric pressure.

The heating mechanism is composed of five electrical feedthroughs, one in the center of the baseplate and the other four in a circle around it, and a copper top piece for attaching the boats. Each of the four boats is suspended between one of the four outer feedthroughs and the center feedthrough. To heat a particular boat, a power supply applies a voltage across the outer feedthrough and the center feedthrough so that a current runs through the intended boat, heating its contents. A switch is used to select the desired boat. Water lines run through the feedthroughs to cool them during evaporation so that most of the heating occurs in the boats.

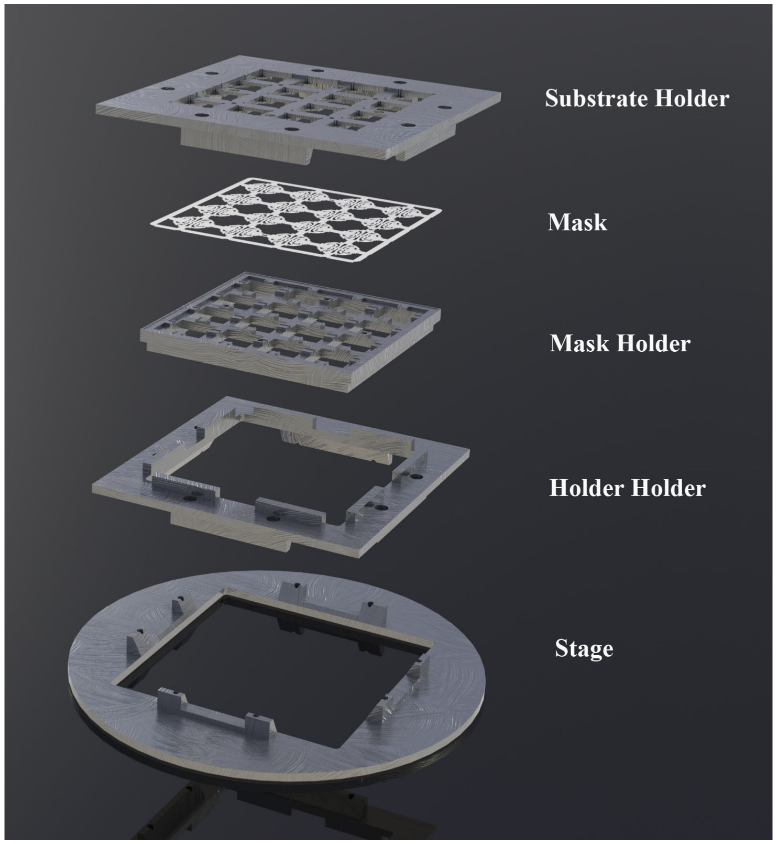

Figure 3-8: SolidWorks representation of mask assembly

3.2.4 Substrate holder and mask assembly

The substrate holder's function is to suspend the substrates above the sources. It holds 16 half inch wafers, each of which rests on four protruding corners slightly below the top the top face of the piece.

The purpose of the mask is to force deposition of evaporated material to occur in a certain pattern. It is held in front of the substrates so that material is deposited in the pattern inscribed on the mask. Our system includes two masks that can be used interchangeably, one for the active layer of a device and one for the top electrode. They are made of a very thin (1 mil) layer of chrome and were made by chemical etching.

The mask assembly is a set of intricate pieces that fit together tightly. It has

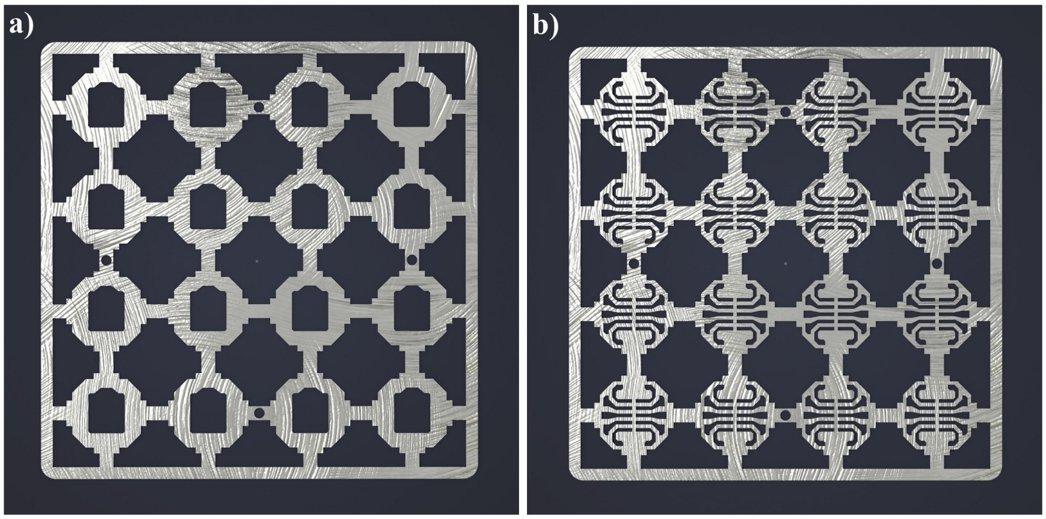

Figure 3-9: SolidWorks representation of a) the organic layer mask and b) the metal electrode mask.

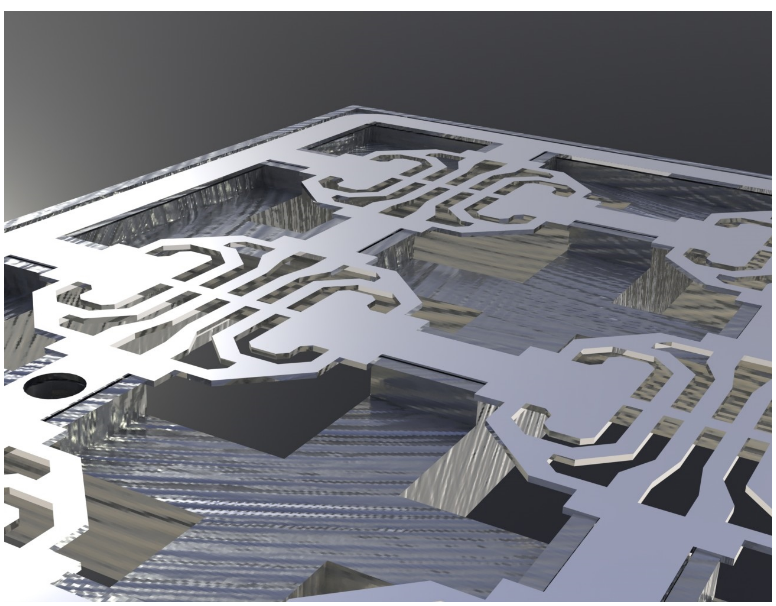

Figure 3-10: The mask is held firmly by the mask holder, suspended by a set of small grooves.

five components: the substrate holder, mask, mask holder, "holder holder," and stage. It sits on top of the substrate rotation system at the top of the chamber and can be moved in and out of the chamber through the top port inside the glove box. Loading the substrates from inside the glove box ensures that thin-film devices never leave the inert nitrogen environment during the fabrication process. All pieces except for the mask are made of aluminum.

The mask is held firmly by the mask holder, suspended by a set of small grooves as shown in Figure 3-10. When the pieces are in place, the surface of the mask lifts the substrates from the substrate holder to ensure accurate placement of the mask pattern. The mask holder fits very tightly into the "holder holder" to make sure that it doesn't shift during evaporation, which would offset its pattern on the substrate. The "holder holder" is separate from the stage so that it can be easily removed from the chamber and replaced.

The stage fits into the top of the rotation mechanism and makes sure that material is only deposited on the substrates. The pieces fit together as shown in figure 3-8, separated by "feet." In designing these pieces, we worked closely with machinist Thomas Liimatainen at Mount Holyoke College. We worked to make the design as easy to machine as possible, which involved rounding all inside corners to accommodate the round drill he used to cut the piece.

3.2.5 Substrate rotation mechanism

The purpose of the substrate rotation mechanism is to hold the mask assembly a specific distance above the evaporation sources, and to rotate the substrates during evaporation to ensure uniform deposition. A ball bearing is suspended from the top flange of the chamber by pieces called "hooks" as shown in Figure 3-11. The outer ring of the bearing fits into a large gear. This allows a wormgear, driven by a motor outside the chamber, to rotate the stage, which fits into a groove in the bearing as shown. A piece called the "collar"

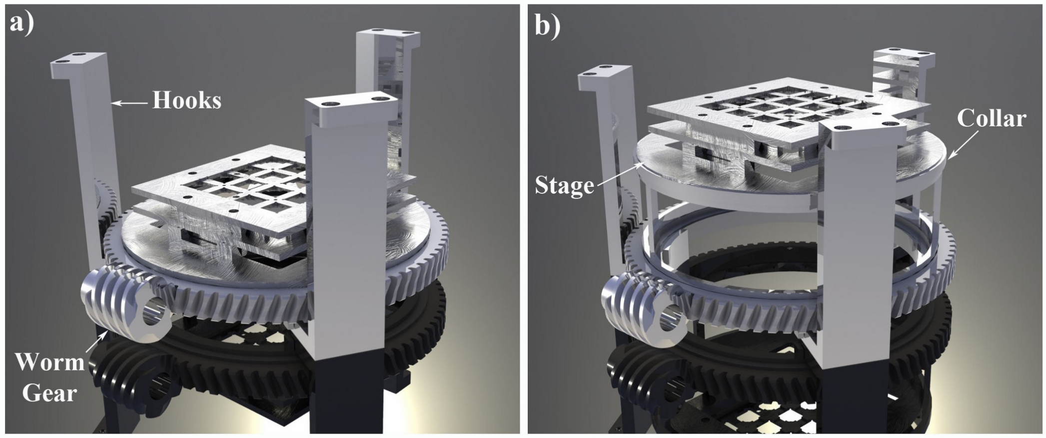

Figure 3-11: SolidWorks representation of substrate rotation mechanism a) without collar and b) with collar.

can be added in order to increase the distance between the sources and the substrates. If this is used, a small metal sleeve is inserted to protect the rotation mechanism and chamber walls from material deposition.

3.2.6 Metal sleeve

The metal sleeve serves the same purpose for the lower section of the chamber as the small metal sleeve serves for the rotation mechanism: it protects the walls of the chamber during evaporation. It is suspended from the bottom of the hooks as shown in Figure 3-12, and can be removed through the bottom opening of the chamber. Though all feedthroughs into the chamber (thickness monitor and shutter) must be removed in order to remove the sleeve, it provides a significant advantage over common cleaning processes. A laboratory worker can remove the sleeve and replace it with a clean sleeve within minutes, then clean the original sleeve without occupying the evaporator.

Figure 3-12: SolidWorks representation of metal sleeve. The sleeve is suspended from the ”hooks” in the substrate rotation mechanism and protects the chamber walls from vaporized material during evaporation.

3.2.7 Shutter

The shutter is located just underneath the substrate rotation mechanism and is operated from outside the chamber using a rotational feedthrough. Its purpose is to block the substrates from vaporized source material before and after desired deposition in order to ensure accurate layer thickness. The feedthrough is operated by an automated switch.

3.2.8 Quartz crystal thickness monitor

The quartz crystal thickness monitor measures the thickness of deposited films. Quartz possesses piezoelectric properties, which means that it experiences mechanical deformation in response to an applied voltage. Applying an alternating current to the quartz crystal will induce oscillations. If the thickness monitor is present in the chamber during evaporation, material will be deposited on the oscillating quartz crystal as well as on the substrates. This causes the resonant frequency of the oscillating crystal to change. This information can be interpreted by the thickness monitor in order to provide information about the amount of material that has been deposited on the substrates.

3.2.9 Vacuum system

Our vacuum system consists of a turbomolecular pump connected directly to the chamber as well as external backing and roughing pumps. Our roughing pump is a "hook and claw" dry pump, which uses two interlocking rotors rotating in opposite directions. The interlocking design traps air in two compartments, one which is open to an inlet port, and one which is open to an outlet port. As the rotors rotate, the location of the inlet and outlet ports change relative to the compartments, so that air in one compartment is compressed into the outlet, while air from the vacuum chamber flows into the other compartment. As the rotation continues, the compartment drawing air from the chamber closes to the inlet and opens to the outlet, allowing the process to repeat. Since there is no contact between the rotating parts during operation, there is no need for lubrication, and consequently no risk of contaminating the air in the vacuum chamber. The hook and claw pump has a very high gas throughput at high pressures but it slows down considerably at a certain point. This makes it very effective for pumping down the chamber directly from atmospheric pressure, but it can only achieve about 10^{-2} torr.

To bring the pressure in the chamber down to operating pressure (10^{-8} or 10^{-9} torr), we use a turbomolecular pump. This pump is capable of achieving very low pressure but has low throughput and therefore cannot operate at atmospheric pressure. It is a momentum transfer pump, and works by spinning a cylindrical column lined with thin metal blades. These blades are shaped so that, as the column spins, they transfer momentum to nearby particles, knock-

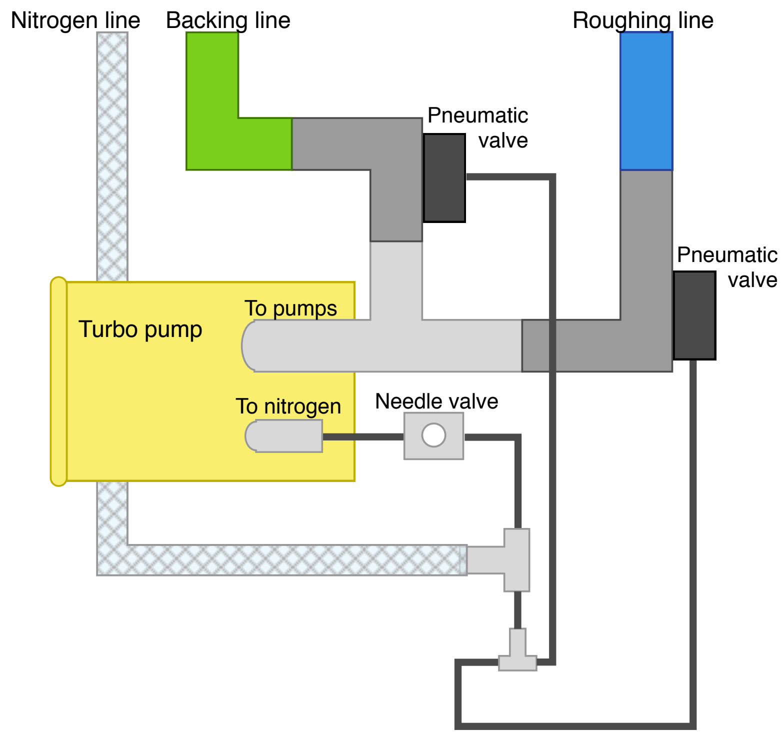

Figure 3-13: Schematic diagram of pumping system. The roughing pump brings chamber pressure down to 10^{-2} torr, the backing pump brings it to 10^{-4}, and the turbomolecular pump brings it to 10^{-8} or 10^{-9} torr.

ing them out of the column. To avoid building up pressure on the backside of the pump (which can cause it to stall), a backing pump must be connected in series behind the turbopump. In contrast, the roughing pump and the turbopump must be connected in parallel, but each pump must act on the chamber independently because they operate at different pressures. The vacuum pump system is diagrammed in Figure 3-13.

Our backing pump is a scroll pump, which uses two intertwined spiral-shaped pieces, one fixed and one rotating. The inlet is located at the opening of the spiral, and the outlet is located at the center of the spiral. As one piece, rotates, the air flowing into the inlet is compressed around the spiral shape and forced out of the outlet. Because the scroll mechanism is tighter and works at a higher velocity, its maximum throughput occurs at lower pressures than the hook and claw. Consequently, it is capable of achieving lower pressures.

The roughing and backing pumps are located outside of the lab, in a supply room across the hall. This saves space inside the lab and improves the working environment by reducing noise. The pumps are connected to the evaporation chamber by tubes that run along the lab's ceiling. The roughing and backing lines are opened and closed by pneumatic valves, which are operated by nitrogen pressure. This means that the valves must be connected to the nitrogen lines in the lab which supply nitrogen to the glove boxes. An electronic switch which uses a solenoid can allow nitrogen to flow into the valve. The turbopump is also equipped with a hand operated needle valve, so that nitrogen can be bled into the chamber when bringing it up to atmospheric pressure.

Rough pressure gauges are connected to the roughing line, the backing line, and the chamber to measure pressure during pump-down. An ion gauge is connected directly to the chamber to measure its pressure once the turbopump is running.

3.3 Building a solar cell

Once the evaporator was assembled, we were able to start fabricating electronic thin film devices. In this section, I will briefly describe the fabrication and characterization of an organic donor/acceptor photovoltaic device.

3.3.1 Device description

The active layers of this device, organic polymers poly(3-hexylthiophen-2,5-diyl (P3HT) and [6,6]-penyl-C61-butyric-adic-methyl,ester (PCBM), are combined in a chemical blend known as a bulk heterojunction. The P3HT absorbs incident photons as well as acting as the hole acceptor (where "hole" means the lack of an electron) while the PCBM acts as the electron acceptor. When a photon excites a P3HT molecule, or causes a valence electron to move to the conduction band, the electron and the vacancy it leaves in the valence band create a bound electron-hole pair called an "exciton." The interface between the P3HT and the PCBM causes the exciton to split, as the hole remains in the P3HT while the electron moves into the PCBM, creating a voltage across the cell.

An ITO layer printed on a half-inch-by-half-inch-by-1 mm glass substrate acts as the anode. A planarization layer of poly(3,4-ethylenedioxythiophene)poly(styrenesulfo (PEDOT:PSS) is included between the ITO anode and the P3HT:PCBM blend to provide a smooth surface. A layer of Ca acts as the anode, followed by a layer of Ag to increase conductivity.

3.3.2 Fabrication procedure

The device fabrication process begins with substrate cleaning. Glass substrates pre-printed with a set of ITO electrodes are sonicated in consecutive ten minute baths of micro-90, de-ionized water, acetone, and isopropanol. They are then transferred into the glove box while immersed in isopropanol where they are dried using pressurized nitrogen gas and stored in isolated Fluoroware compartments. Next, 50 mL of PEDOT:PSS are deposited on the substrate by spin coating at 500 rpm, followed by annealing at 150 degrees C for 5 minutes. Then 35 mL of P3HT:PCBM are deposited by spin coating at 600 rpm and annealed for 10 minutes at 110 degrees C. The annealing caused the P3HT to preferentially separate from the PCBM so that a very thin layer of pure P3HT forms next to the anode, facilitating charge transfer. Finally, 25 nm of Ca and 80 nm of Ag are consecutively deposited by evaporation, using the thermal evaporator described in this chapter.

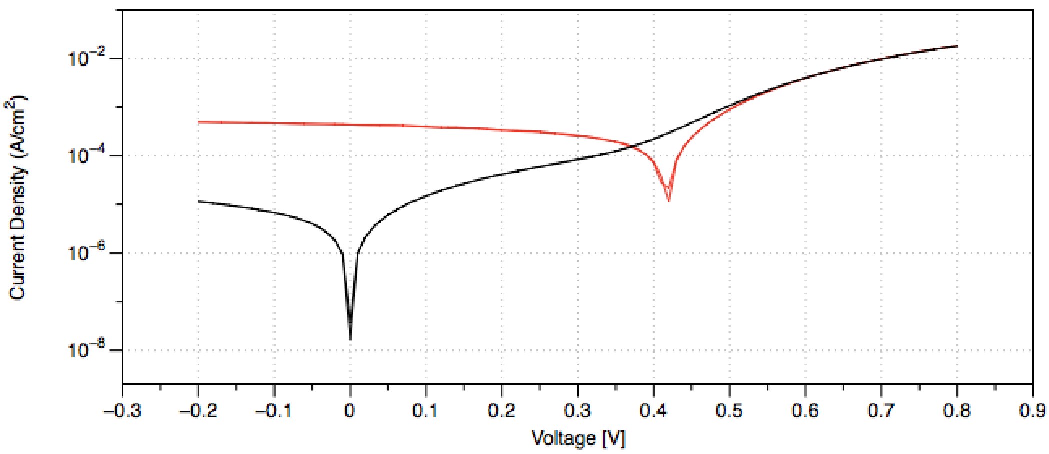

Figure 3-14: Log/linear current-voltage curve for a photovoltaic device fabricated using the thermal evaporator described in this chapter.

3.3.3 Characterization

Once fabrication is complete, the device is characterized. This involves applying a voltage across the device's terminals and sweeping it from -.2 V to +.8 V while a LabView program records and processes current-voltage characteristics. A current will flow through the device in response to a bias even if no light is shining on the device. When the device is illuminated, a combination of dark current and photocurrent, or current generated by the device structure, flows through the device. This current is referred to as light current. Consequently, the device is tested first in the dark to generate a dark IV curve and then under the light of a solar simulator to generate a light IV curve.

Figure 3-14 shows a log/linear IV curve of the device, in which the current density is scaled logarithmically. The device's dark current is shown in black and its light current is shown in red. The short-circuit current density (Jsc), or the current per unit area through the cell when the anode and cathode are directly connected in a short circuit, is shown where the light current plot crosses the y-axis (V=0). The open-circuit voltage (Voc), or the voltage across the device when its anode and cathode are not connected, is shown at the minimum point of the light current.

The short-circuit current density of the device shown is about .6 mA/cm2 and its open-circuit voltage is .42 V. Our characterization station is not yet complete, so we are currently unable to calculate our solar cell efficiencies. However, the highest short-circuit current density our lab has achieved is 3 mA/cm2, and the highest open circuit voltage we have achieved is .53 V. Shrotriya et. al. achieved a short-circuit current density of 9.996 mA/cm2 and an open-circuit voltage of .6028 V.

3.4 Discussion

Construction of the evaporator was completed last spring and it has been operating smoothly since then. We estimate the total cost of the system, with all parts new, to be less than $40K. It takes less than 3 minutes to reduce the pressure in the evaporator chamber from atmospheric pressure to operating pressure, and deposition takes less than 10 minutes. Switching out a dirty metal sleeve for a clean one takes about 15 minutes.

Though the system did achieve our goals of low construction cost, quick and easy operation processes, and simple cleaning processes, it could be improved in several ways. First, the base plate warps slightly when the chamber is closed, which somewhat compromises the seal between the base plate and the bottom chamber lip. Increasing the thickness of the base plate might improve the seal.

Second, the protective metal sleeve is somewhat difficult to attach to the bottom of the "hooks" in the substrate rotation mechanism, since the attachment point is not visible from outside the chamber. A better design should use magnets to connect the sleeve to the bottom of the "hooks," since this would require much less manipulation by the laboratory worker.

An additional viewport would make interior components of the evaporation chamber more visible and help laboratory workers confirm that the evaporation process was working. With an additional viewport, a laboratory worker could shine a light through one viewport while looking through the second viewport in order to better see vaporized material. The existing viewport is also inconveniently small.

The switch that allows laboratory workers to choose among the four source boats in the chamber is also inconveniently large. It might almost have been more space efficient to use four power supplies, one for each of the boats. A smaller switch would have allowed more controls to fit in the electronics rack to the right of the glove box.

The base plate elevator system is slightly difficult to operate as well. The base plate does rise along the post as the wheel at the top of the post turns, but if the wheel is released, the base plate falls back down to the bottom of the post. This makes it difficult for a laboratory worker to secure the base plate in the closed position, because he or she must hold it flush with the bottom lip of the chamber while securing it with the clamps. A better design would hold the base plate in place above the bottom of the post without anyone there to hold it. A rack and pinion elevator device is a possible solution to this problem. The spring at the bottom of the elevator post is also inadequate to catch the base plate when it falls, and we haven't been able to find a spring which will adequately oppose the force of the falling base plate. A pneumatic system might be more effective for this purpose.

Last, the design would have been improved by restricting the system to a specific width limit below the glove box. As we will see in Chapter 4, protruding evaporator components severely limit the width of the sputtering system that we have also designed for this project, which is located to the left of the evaporator, under the same glove box. If this problem is compounded by the sputtering system, our plan to eventually include a third apparatus under the glove box might be difficult to implement.

Chapter 4

Sputtering system design

This chapter gives a detailed account of our sputter system design process. I will begin with a literature review of existing low-damage sputtering techniques and then provide a detailed component-by-component description of our novel design. I will end with a discussion of our design's success in terms of low cost, usability, and substrate protection.

4.1 Existing low-damage sputtering techniques

Sputter deposition systems today possess the same drawbacks as evaporators: complicated and time-consuming operating procedures, high cost of construction, and laborious maintenance procedures. Recently, the process has developed a new problem. The fabrication of many semiconductor devices involves deposition by sputtering onto a substrate previously coated with an organic thin film. However, energetic particles in the sputtering plasma have been shown to cause critical damage to organic layers during sputter deposition by destroying carbon-based bonds in the material. This creates micro-current paths through the organic layers which degrade device performance [16]. The magnetic field in the planar magnetron configuration protects substrates to some extent, but a significant amount of damage still occurs. This section reviews four different methods for further protecting underlying organic layers during magnetron sputtering: Hyper-thermal Neutral Beam sputtering (HNB), Kinetic Energy Controlled deposition (KECD), a Cylindrical sputtering module, and Facing Target sputtering (FTS).

4.1.1 Neutral Beam Sputtering

Hyper-thermal Neutral Beam sputtering (HNB) [4] or Neutral Particle Beam Assisted sputtering (NBAS) [10] is a low-damage sputtering technique consisting of an inductively coupled plasma source (which generates a plasma using a time-varying magnetic field), two parallel facing magnetron sputter guns, and reflector. The magnetron sputter guns supply elements of target material to the inductively coupled plasma where they become ionized. These ions are then accelerated into a metal reflector positioned perpendicular to the sputter sources which neutralizes the ions by Auger neutralization and accelerates them towards substrates situated across the sputtering chamber from the reflector (see Figure 4-1). Some HNB systems employ a magnet limiter [4], which is an array of permanent magnets positioned between the plasma and the substrates in order to confine the plasma and decrease bombardment of the substrates by high energy particles.

Lee et. al. [4] reported low leakage current density at reverse bias (no actual numerical data provided) of OLEDs fabricated by HNB sputtering, indicating that underlying organic layers were not damaged. UV exposure tests further confirmed this conclusion. However, the device exhibited poor turn-on characteristics which were attributed to iron impurities generated by the sputtered stainless steel reflector.

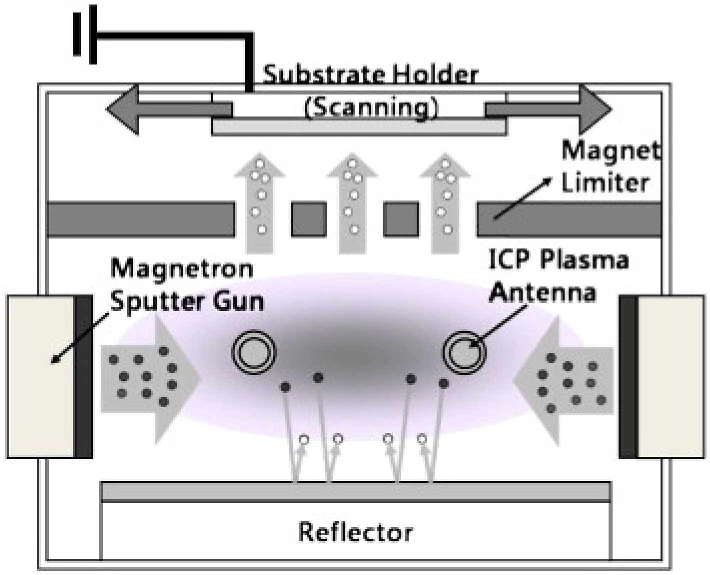

Figure 4-1: Cross-sectional view fo the HNB ITO sputtering system [4]

4.1.2 Kinetic Energy Controlled Deposition

Kinetic energy controlled deposition (KECD) [19, 20, 5] is a low-damage sputtering method that uses a conventional magnetron sputtering source but separates the substrates from the sputtering source by a grounded grid electrode. This grid electrode makes it possible to control the kinetic energies of sputtered particles along with their incidence angles to the substrate during the film forming process (see Figure 4-2). ITO films with resistivity as low as 3.5×10^{-4} Ohm-cm and very smooth surfaces can be produced by KECD [19] and deposition rates as high as 50 nm/min [5] can be achieved. Yamada et. al. [5] reports damage inflicted on the organic layer, measured by degradation of photoluminescence intensity, while using a .1 T permanent magnet rather than the usual .02 T as well as a grounded grid electrode. It was found that the peak of the PL spectrum of the organic film (Alq_3, 80 nm thick) after exposure to plasma at RF 150 W for 600 seconds was still only about 45% of the peak before exposure to plasma, and the peak of the spectrum after plasma

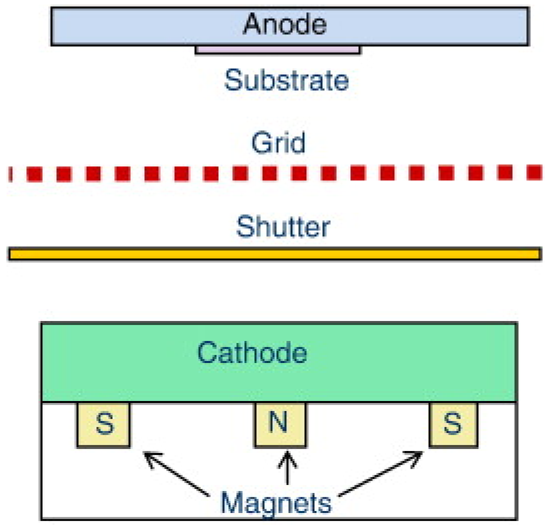

Figure 4-2: Diagram of the KECD set-up with grid electrode [5]

exposure at RF 350 W for 833 seconds was only about 35% of the peak before plasma exposure. However, after actual deposition of a 200-nm-thick AZO film on the 80-nm-thick Alq_3 film at RF power 350 W, the peak of the PL intensity spectrum was about 75% of the peak before deposition, indicating that organic layers were damaged less during actual sputter deposition than during exposure to plasma. This is attributed to protection of the organic layers by deposited film. An AZO film with resistivity of about 1.1×10^{-3} Ohm-cm and transparency higher than 90% above wavelength of 400 nm was achieved. This data indicates that the KEDC method with high magnetic field and grounded grid electrode is an effective sputtering method which reduces damage to underlying organic layers during deposition. However, a significant amount of damage still occurs. It is suggested that the damage may be further decreased by controlling the voltage of the grid electrode.

4.1.3 Cylindrical Sputtering Module

The cylindrical sputtering module [6, 21, 22] employs a cylindrical magnetic target from the bottom of which Ar and O_2 gases are supplied. Plasma is generated inside the target by RF magnetron excitation and confined within the target, below substrates which are positioned perpendicular to the cylinder walls (see Figure 4-3). Yamamoto et. al. [6] Reported a device fabricated by this method with a current density of 883 mA/cm^2 at an applied voltage of 10 V and a maximum external quantum efficiency of 0.76 percent. However, the deposition rates are very slow, [21] e.g. 1.62 nm/min at 50 W, and 6.66 nm/min at 200 W [6]. It seems that a fairly high deposition rate could possibly be achieved at a very high power.

This method is investigated least in the literature of the four addressed in this paper. Though it seems to be an effective method for protecting underlying organic layers, the information available isn't thorough enough to provide an accurate idea of the technique's practicality.

4.1.4 Facing Target Sputtering

Facing Target Sputtering (FTS) seems to be the most widely used and thoroughly investigated sputtering method for protecting underlying organic films on substrates, and has been cited as the most effective method for this purpose [12, 23]. This method introduces a configuration of vertically parallel facing targets with a substrate holder perpendicular to the target plane (see Figure 4-4). This design effectively traps the plasma between the magnetized target planes, confining it to the region below the substrates so as to reduce collisions of gaseous ions with the substrates. FTS is capable of producing thin multilayer films as well as alloy films and dependence on parameters such as inter-target distance, pressure, and substrate-to-target distance has been investigated [24]. Most instances of FTS deposition in the literature use DC

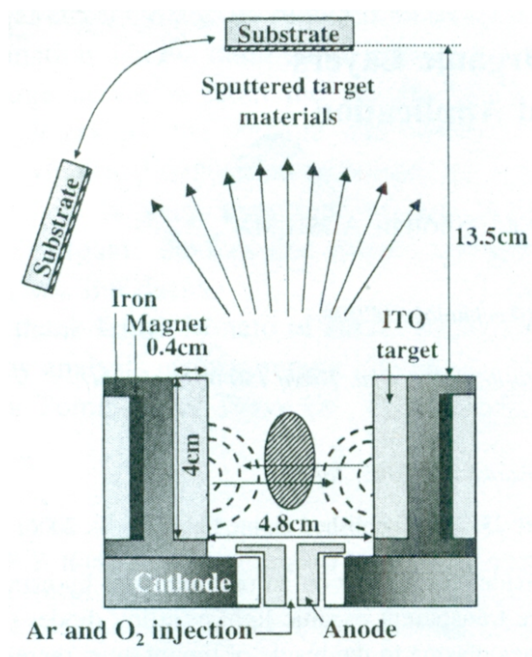

Figure 4-3: Cross-sectional view of cylindrical target structure [6]

sputtering but RF sputtering is also possible [25, 26, 23]. However, Matsuoka et. al. [26] reports that ion bombardment of a film surface is more problematic during RF FTS than DC FTS due to the higher plasma potential present in RF FTS, though this ion bombardment can be suppressed when RF sputtering is performed at higher sputtering gas pressure and input power.

Kim et. al. reports Al films grown on NPB/Alq_3 films with leakage current density as low as 1×10^{-5} mA/cm^2 at reverse bias of -6 V [7] and ITO films grown on organic and LiF films with leakage current density as low as 9.2×10^{-5} mA/cm^2 at reverse bias of -6 V [27]. However, both these methods involve the deposition of a thin Mg-Ag buffer layer on the organic films before sputter deposition by FTS.

Several techniques have been invented in order to avoid the use of these buffer layers. Kim et. al. [28] directly sputtered an Al cathode on LiF/Alq_3 in a mixture of Ar and Kr in order to produce a device with leakage current density of 1×10^{-5} mA/cm^2 at -6 V (the same as that of the aluminum device

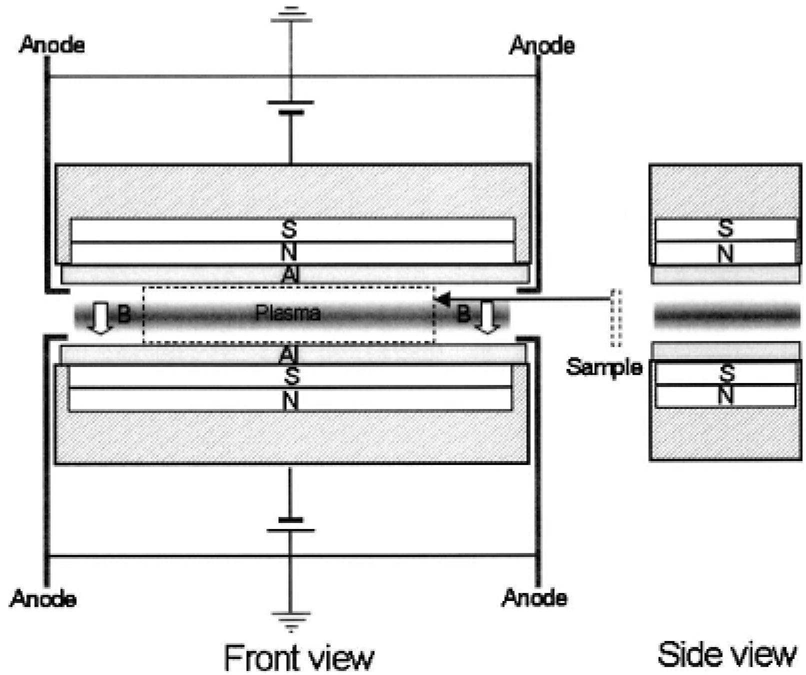

Figure 4-4: Schematic diagram of an FTS system and sample position, vertically located to the targets [7]

deposited with a buffer layer by Kim et. al. [7]). However the development of FTS with ladder-type-magnet arrays by Moon et. al. [12] made this mix of gases unnecessary. In this system, additional permanent magnets are inserted in the center region of the sputtering gun, improving the uniformity of the magnet field between the targets and creating a higher density plasma at the center region of the gun (see Figure 4-5). Devices with Al cathodes deposited directly on organic layers exhibited leakage current densities as low as 5×10^{-6} mA/cm^2 at -6 V (lower than that achieved with the mix of gases [7]). This method has been studied in depth and films made of ITO, IZTO, and various multilayers grown by this method have been characterized [8, 29, 30, 31].

Onai et. al. [22] introduces a two-step FTS deposition method that avoids the use of a buffer layer in the deposition of ITO on a 40-nm-thick BAlq layer by depositing the first 20 nm of the target material at a low rate

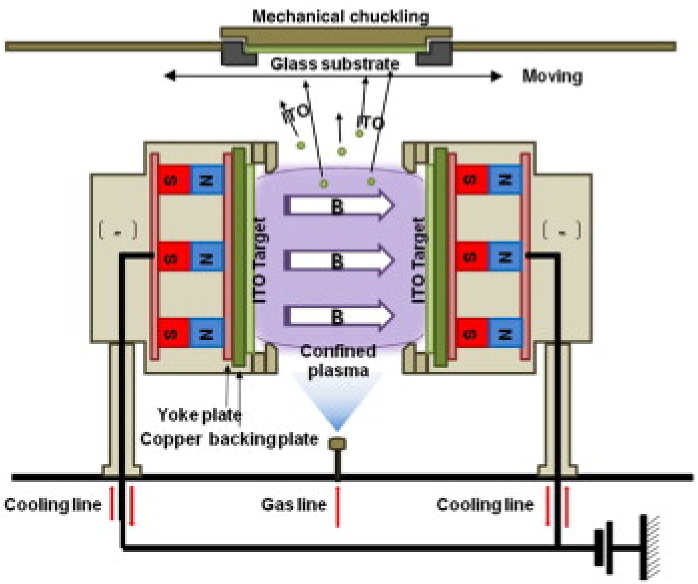

Figure 4-5: Schematic diagram of a linear-facing target sputter gun with a ladder-type magnet array [8]

of 5 nm/min (50 W) and the rest of the layer at 44 nm/min (200 W). Damage inflicted on the organic layer during the deposition process was measured by degradation of photoluminescense (PL) intensity of the Balq. The peak PL intensity of the device sputtered at 200 W was about 28% of peak PL intensity of an unsputtered device, while the peak intensity of the device sputtered at 50 W was about 63% of the peak intensity of the unsputtered device. However, the peak intensity of the device fabricated by the two-step method was also about 63% of the peak intensity of the unsputtered device (the same as that of the device sputtered entirely at 50 W), proving that the two-step process is an excellent way to reduce damage to organic layers without significantly reducing deposition rate. The degradation in PL intensity of the organic layer after deposition is slightly more significant in this model than in the KECD model with grounded electrode [5]. However, many parameters of the two experiments differ, such as the organic material, the sputter-deposited material, and the thicknesses of each of these films. Regardless, it seems like these two

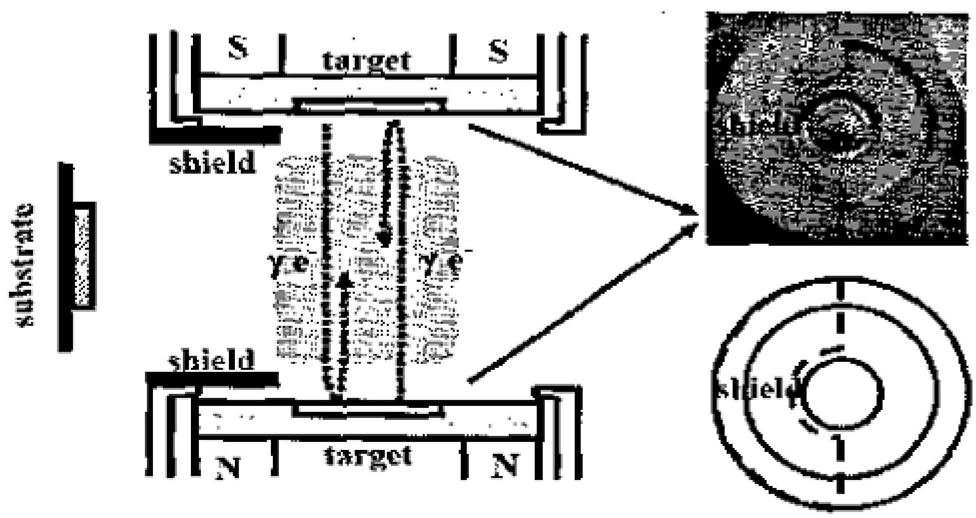

Figure 4-6: Schematic configuration of FTS with shield mounted on targets [9].

methods provide comparable protection for underlying organic films during deposition.

Lei et. al. [9] examines one more method for avoiding the use of a buffer layer. In this FTS model, a sector-shaped metal shield is inserted near the target electrode in order to reduce damage to a 40-nm-thick BAlq layer during the deposition of a 150-nm-thick ITO electrode (see Figure 4-6). Damage was again measured by degradation of PL intensity of the BAlq. In this case PL measurements without the shield were about the same as those cited by Onai et. al. [22] However, using the shield, the peak intensity of the device sputtered at 200 W was about 82% of the peak intensity of an unsputtered device, while the peak intensity of the device sputtered at 50 W was about 87% of the peak intensity of the unsputtered device. It is believed that the significant improvement of PL intensity caused by the insertion of the shield is mainly due to the removal of secondary-electrons incident to the substrate. This shows that the FTS system aided by a sector shaped shield is more effective for protecting organic layers on substrates than the two-step FTS model or possibly the KECD model with grounded grid electrode.

4.2 Novel sputtering system design

Our novel sputter system design attempts to address the same problems as the evaporator (size, expense, and inconvenience), while also decreasing substrate damage by energetic particles. We incorporated as many features of the evaporator into the sputtering system design as possible, while also taking advantage of the facing target configuration described in Section 4.1.4 and the sector-shaped target shields proposed by Lei et. al. Our own novel low-damage feature, an array of magnets to extend the field above the target region, has been incorporated into the design as well. We expect the system to be built by the end of the summer, at which point we will perform tests to evaluate its low-damage capabilities.

I will now provide a detailed description of each of the design's components, as I did for the evaporator. These include magnetron sputter guns, chamber, retractable base plate elevator system, substrate rotation system, metal sleeve, shutter, thickness monitor, and vacuum system. All system CAD designs were created in SolidWorks 2010.

4.2.1 Magnetron sputter guns

The design of the system as a whole was largely determined by the magnetron sputter guns. Several factors constrained their design. First, for a single source material, we needed two guns in the facing target configuration, as described in Section 4.1.4. We chose this method because the studies reviewed in Section 4.1 indicated that it was the most consistently effective and well understood of the known low-damage sputtering methods. Furthermore, it is possible to

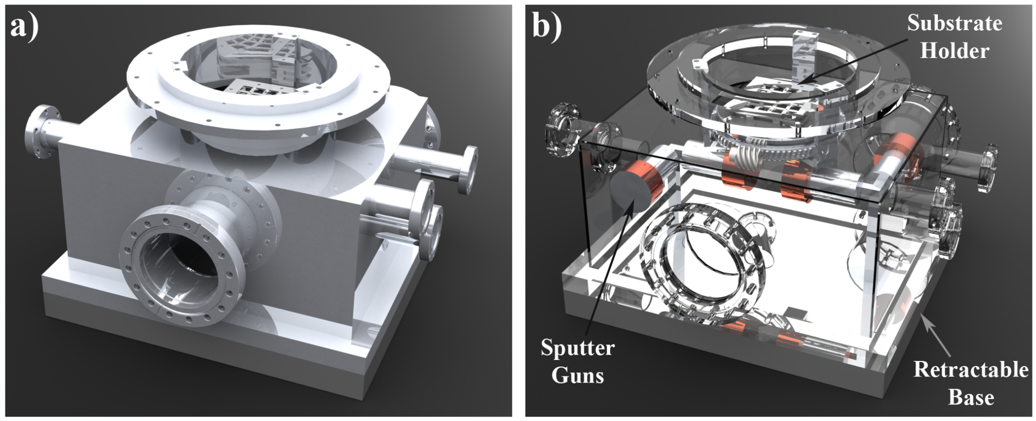

Figure 4-7: a) SolidWorks representation of sputtering chamber. b) SolidWorks representation of sputtering chamber with substrate holder, sputter guns, and base plate shown.

arrange commercially ordered sputter guns (with a few modifications, as described below) in this configuration, whereas many of the other methods would have required elaborate custom designs. Using the facing target method meant that we needed the non-traditional magnet configuration shown in Figure 4-8, in which the magnetic field is perpendicular to both gun faces. The polarity of the magnets also had to vary from gun to gun. This can be achieved using the conventional sputter guns described in Section 2.3.3 by flipping one of the ring magnets in the gun head so that the fields of both magnets are oriented in the same direction.

Second, we wanted to attach the guns to the retractable base plate so that they would be as easily accessible as the substrate heating mechanism is in the evaporator. In order to do this while also keeping the guns in the facing target configuration, we needed to mount the gun heads on 90-degree-elbow shafts as shown in Figure 4-9.

Third, our system needed to be capable of multilayer deposition, that is, deposition of multiple films back to back without opening the chamber. In order to achieve this, we added a second gun head on the same shaft, per-

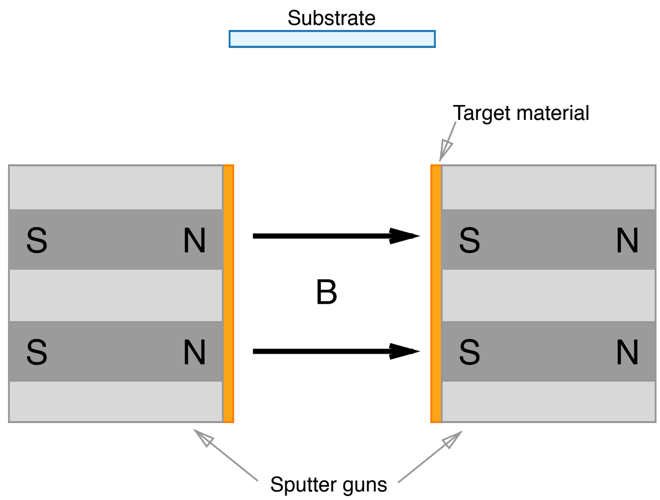

Figure 4-8: Schematic diagram of the non-traditional magnet configuration used in facing target sputtering.

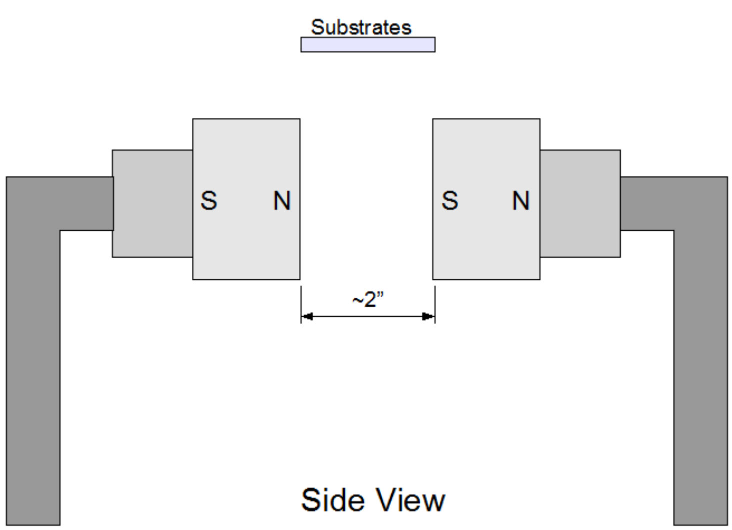

Figure 4-9: In order to attach the sputter guns to the retractable base plate while keeping them in the facing target configuration we mounted the gun heads on 90-degree elbow shafts.

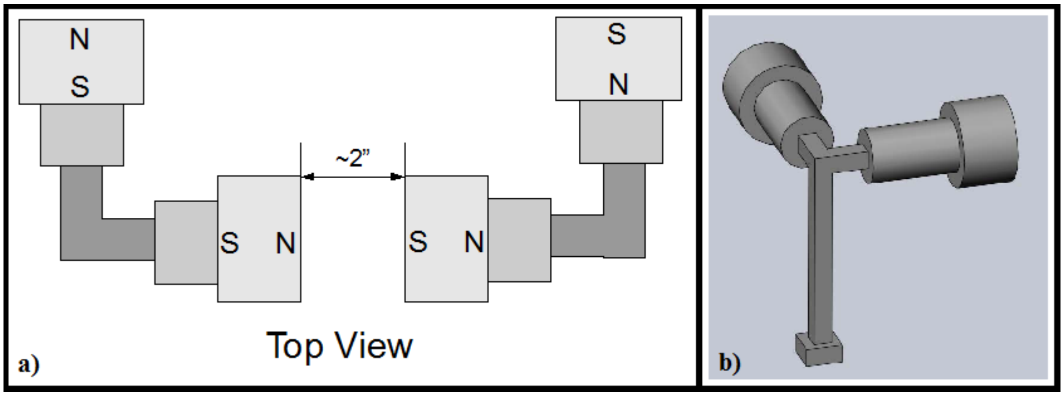

Figure 4-10: In order to perform multilayer deposition, we added a second gun head on the same shaft, perpendicular to the first one. The two shafts will be rotatable from outside the chamber. a) shows a top view schematic diagram of the gun set-up and b) is a concept drawing of the custom design.

pendicular to the first one, as shown in Figure 4-10. The two shafts will be rotatable from outside the chamber and automated by a computer controlled rotation mechanism.

Last, the size constraints on the chamber limited the gun design. The sputtering chamber will be mounted underneath the same glove box as the evaporator, to its left. Eventually we will build a third apparatus that will occupy the space under the glove box to the left of the sputtering chamber as well. This means that the chamber must be less than 15 wide. Space limitations are described in more detail in the next two sections.

One drawback of mounting the gun heads on 90-degree-elbow shafts was that it forced us to fix the target-to-target distance. This choice involved considerations of system size, film uniformity, and plasma confinement. As mentioned earlier, keeping the chamber size reasonably small required the width of the targets to be less than or equal to 2". According to the cosine distribution law described in section 2.2, the film deposited directly above the vaporizing source will be thicker than the film a horizontal distance away from this point. This means that if the source is centered below the substrate, film

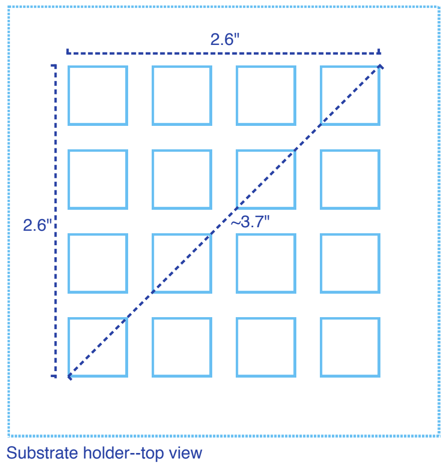

Figure 4-11: For uniformity considerations, the relevant width of the substrate is the diagonal length of the total area occupied by the substrates.

uniformity will be maximized when the source width is equal to the substrate width. In our system, the relevant substrate width is the diagonal length of the total area occupied by the substrates, which is equal to 3.7", as shown in Figure 4-11. Consequently, we chose to use 2" targets, since they were the widest that could fit in the chamber.

Like the evaporator, our sputtering system is equipped with a substrate rotation mechanism. As viewed from above, our sputter guns create a rectangular deposition cross section with width equal to the target width, and length equal to the target-to-target distance, as shown in Figure 4-12a. Deposition on the substrate will happen outside of this region but, as noted above, the amount of material deposited falls off with distance from the source. In contrast, the film directly above the deposition cross section should be fairly uniform.

If the target-to-target distance is small relative to the target width, a small circular region of thick, uniform film will be formed in the center of the substrate as it rotates, as shown in Figure 4-12b. As the target-to-target distance increases, this region becomes larger, making the film more uniform. The size

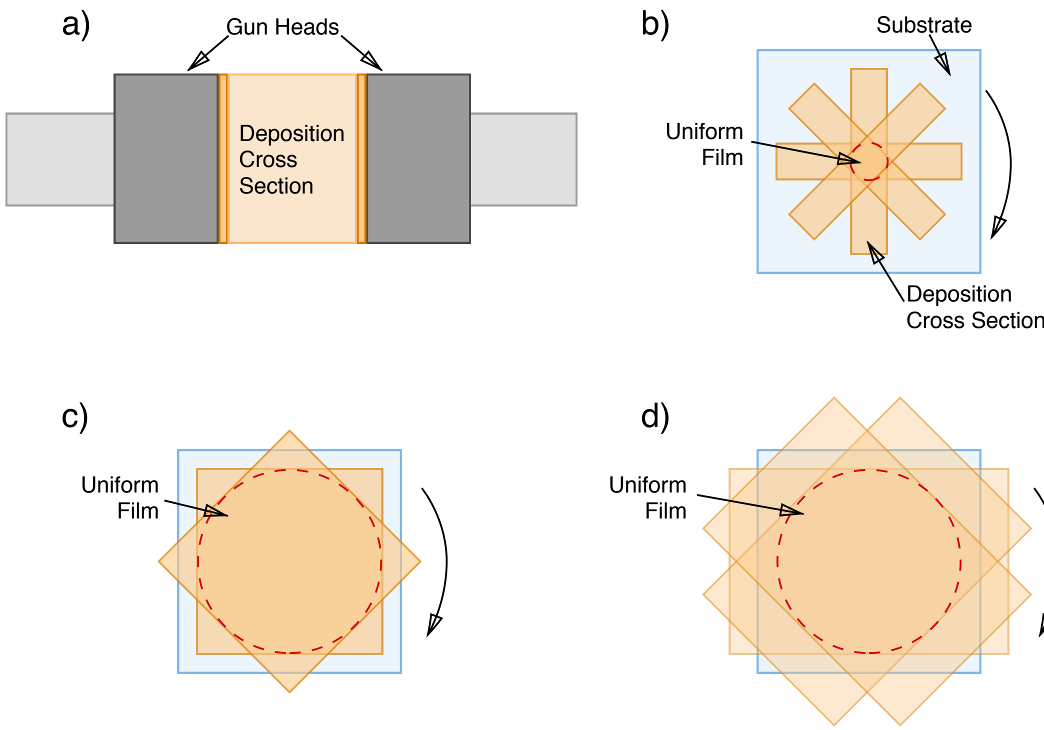

Figure 4-12: a) The deposition cross section of our sputter guns is a rectangle with width equal to the target width and length equal to the target-to-target distance. b) If the target-to-target distance is small relative to the target width, a small region of thick, uniform film will form at the center of the substrate as it rotates. c) The size of this center region is maximized when the length and width of the deposition cross section are equal. d) The size of the uniform center region stops increasing as the target-to-target distance grows wider than the target width.

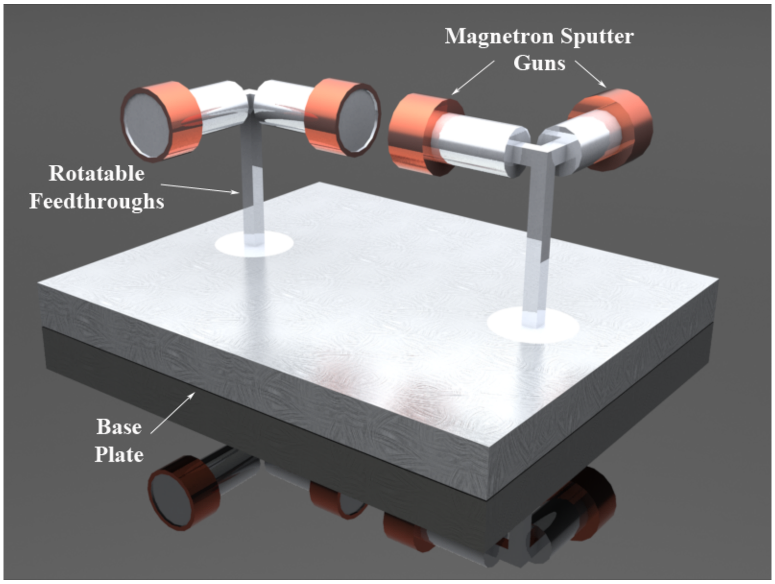

Figure 4-13: SolidWorks representation of base plate with sputter guns and rotating shaft shown.

of this region is maximized when the target-to-target distance is equal to the substrate width as shown in Figure 4-12c. Even if the target-to-target distance increases past this point, the size of this central region does not change, since the overlap of the deposition cross sections at different points in the rotation can only be as wide as the target width, as shown in Figure 4-12d. Since the strength of the magnetic field between the sputter guns decreases as target-to-target distance increases, the optimal target-to-target distance is equal to the target width, which, in our case, is 2." The extra molecules present in the chamber during sputtering cause the vaporized source molecules to scatter before reaching the substrate, which will increase uniformity.

Co-deposition is possible by using a different target material on the left gun of the operating pair than on the right. Because the two materials have different impedances, this requires the use of two power supplies, one connected to each gun, 180 degrees out of phase. Cross-contamination must also be considered, but foreign particles deposited on the target can be removed

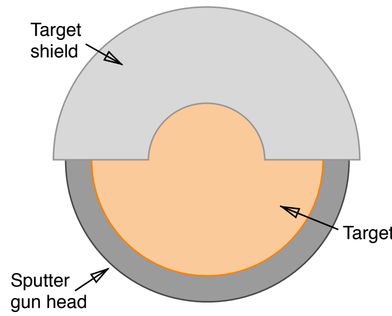

Figure 4-14: Schematic diagram of shield targets proposed by Lei et. al. in order to block ejection of high energy secondary electrons from the edge of the target closest to the substrates.

by pre-sputtering before deposition.

Our design also includes the sector-shaped target shields proposed by Lei et. al., which are diagrammed in figure 4-14. These will most likely clip onto the target face, though this attachment mechanism is yet to be designed.

4.2.2 Chamber design

We designed the sputtering chamber to be as small as possible while still leaving room for the sputtering guns. In order to save as much space as possible we decided on a box shaped chamber rather than a cylindrical one. However, the sputtering chamber features the same top flange as the evaporator chamber, and the same hinged port, which allows access to the top opening of the chamber from inside the glove box.

As mentioned in Section 4.2.1, the chamber's position under the glove box imposes strict size limitations. Not only is the chamber width restricted to 15", but the height of the chamber is a concern as well. The space below the glove box is only 29" high, and the sputter gun feedthroughs will extend below the base plate and attach to the gun rotation mechanism. In order to take advantage of the retractable base plate design we used for the evaporator, the height of the chamber cannot be too large or these parts might not

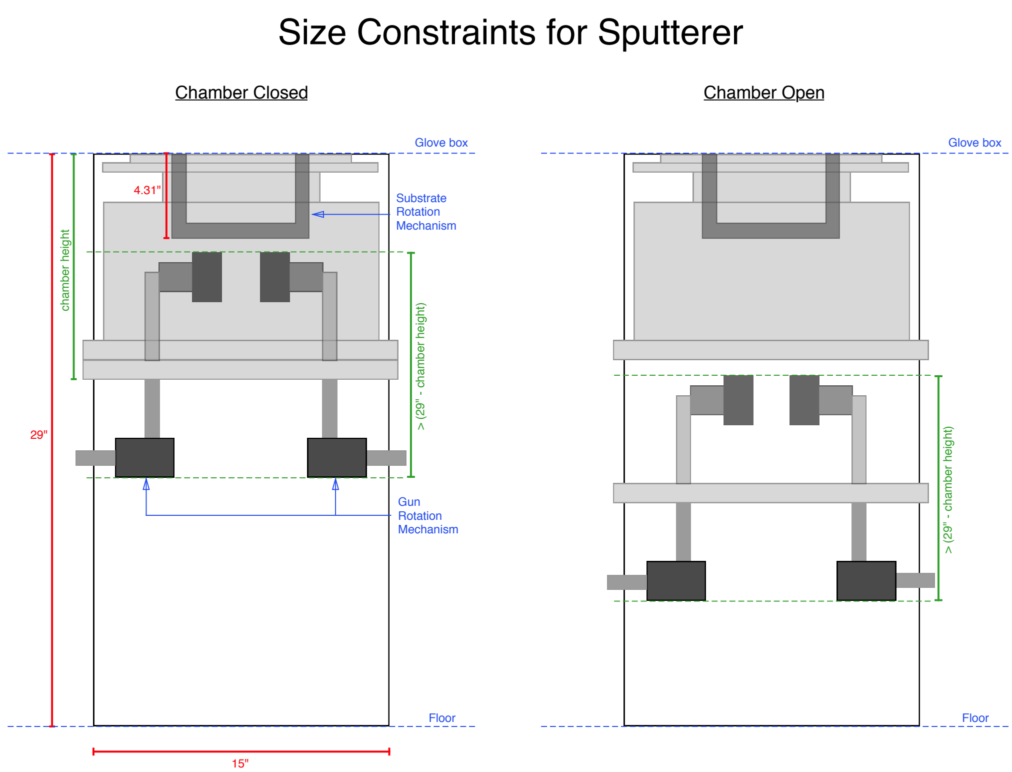

Figure 4-15: Diagram depicting size constraints on the sputtering system imposed by its location underneath the glove box.

fit below the base plate when it retracts. These concerns are summarized in Figure 4-15. The chamber is 15” wide, 12” long, and 10.94” tall, not including the 2” base plate. As in the evaporator, the substrate-to-target distance can be modified, so that it effectively ranges from 1.895” to 3.675.”

4.2.3 Retractable base plate elevator system

Like the evaporator chamber, a retractable base plate elevator system will enable access to the sputtering chamber from outside the glove box through the chamber floor. The .97” evaporator base plate was warping slightly when the chamber was closed, which was compromising the seal somewhat. For this reason, the sputtering system’s base plate is 2” thick, making it both thicker and wider than the evaporator’s base plate. This means that it will be significantly heavier, and so its elevator system will require two posts, one on each side of the sputtering chamber.

The elevator mechanism is yet to be designed, but we expect that the base plate will be permanently attached to one post of the elevator system and clipped to the other. A hinge on the post with the permanent attachment will allow the base plate to swing outward for easy access to the sputter guns when it is unclipped.

4.2.4 Magnetic substrate protection apparatus

The substrate holder and mask assembly in the sputtering system are exactly the same as those in the evaporator. This makes consecutive layer deposition with the two systems very easy, since the same substrate holder can simply be moved from one system to the other without repositioning the substrates.

The substrate rotation mechanism is also very similar to that of the evaporator but with an added feature. The sputter system includes an extra set of stackable pieces which will implement a novel idea for substrate protection. In

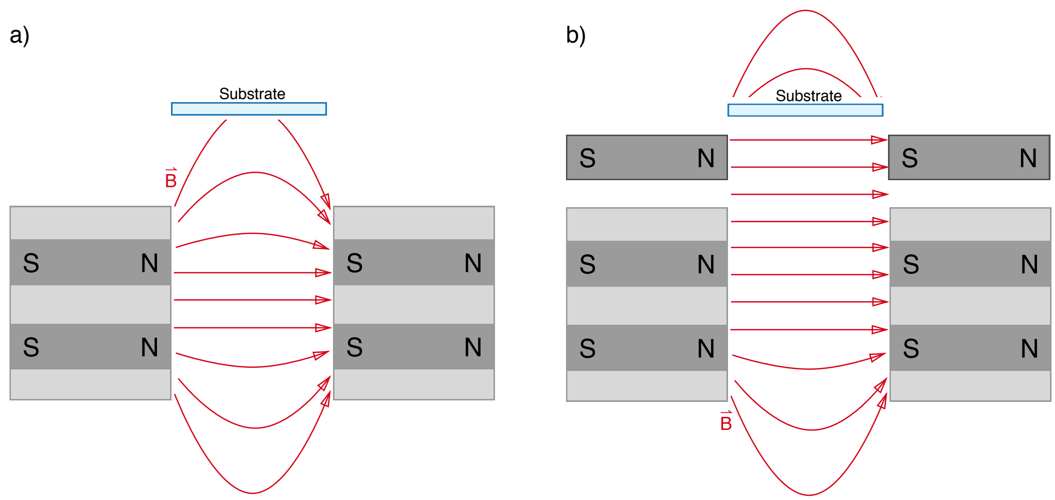

Figure 4-16: a) The magnetic field generated between the sputter guns weakens towards the edges of the targets and the field lines begin to bend toward the substrates. A charged particle traveling along one of these lines will not be affected by the Lorentz force and will have a clear path to the substrates. b) We predict that adding additional high strength magnets between the sputter guns and the substrates will increase the field strength and straighten the field lines near the substrates, protecting them from charged particles that escape the dense plasma region between the targets.

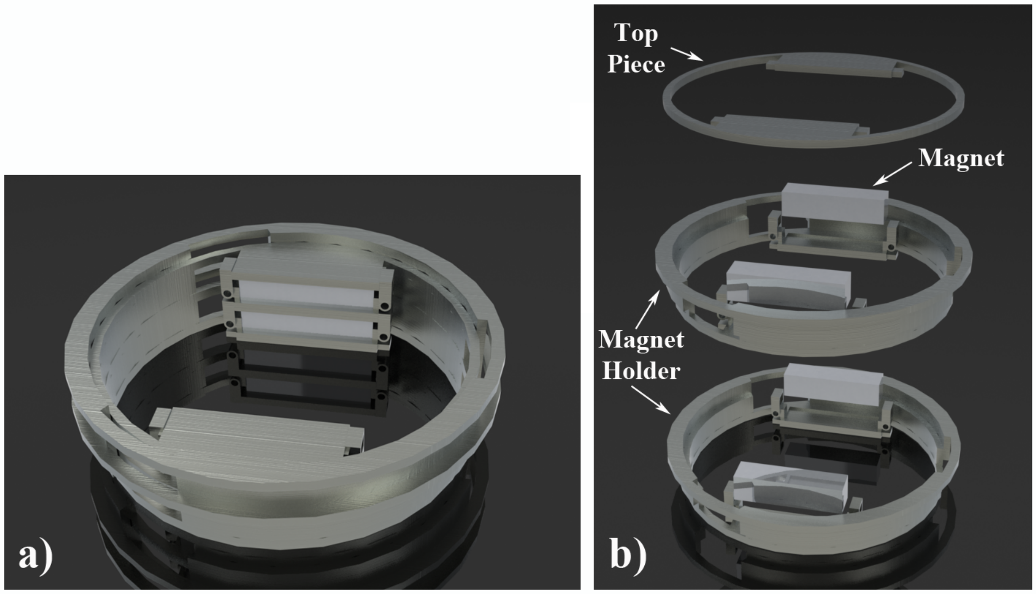

Figure 4-17: SolidWorks representation of stackable pieces used to hold additional high strength magnets on either side of the substrate rotation column.

the facing target configuration, fringing occurs at the edges of the magnetrons, so that the magnetic flux lines bend towards the substrates as shown in Figure 4-16a. An electron traveling parallel to these flux lines will not be affected by the Lorentz force, and hence will have a clear path to the substrates. In an attempt to correct this problem, we have added a magnetic field between the targets and the substrates as shown in Figure 4-16b, parallel to the field generated by the sputter guns. In effect, this will extend the magnetic field above the plasma generation region, so that even if charged particles escape the region of dense plasma between the targets, they will be trapped below the substrates by the Lorentz force.

In order to achieve this, we designed a set of stackable pieces to hold high strength permanent magnets on either side of the rotation column, as shown in Figure 4-17. Each piece includes hinges on either side of each magnet to connect the piece to the one directly above it. The repulsion between adjacent magnets ensures that the hinges will stay in place. A top piece provides an

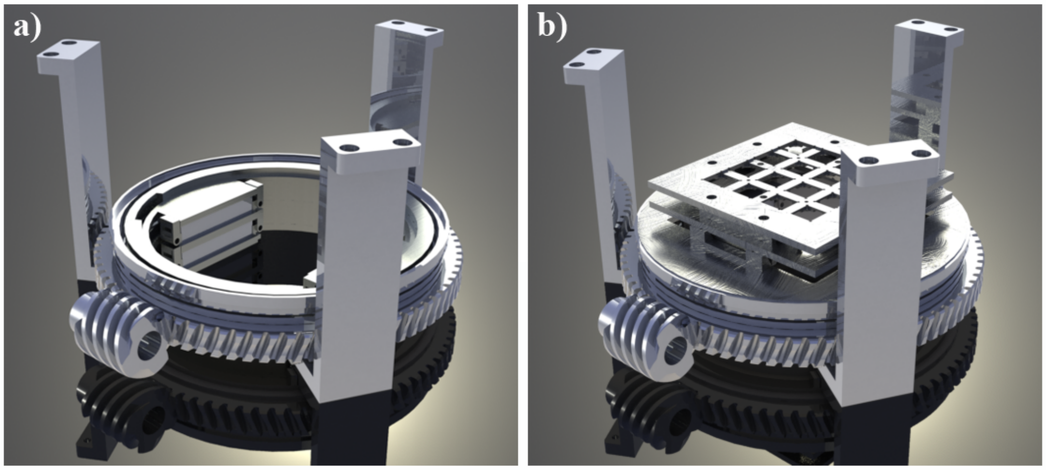

Figure 4-18: SolidWorks representation of the substrate rotation mechanism which shows how a) the magnet holding apparatus is held in place by the hooks b) underneath the substrate holder and mask assembly.

attachment point for the hinges at the top of the stack.

In order to allow as uniform deposition as possible, we moved the extra magnets as far apart from each other as possible. Though ideally the distance between the magnets would be equal to the diagonal length of the region occupied by substrates (3.7"), we could only manage 3.1", since the smallest we could realistically make the magnets was 2"x0.5"x0.5", and the hinges that hold the pieces together required extra room.

We conducted simulations using Maxwell 3D to ensure that the magnetic field generated by the extra magnets would behave the way we expected. These are shown in Figure 4-19. They show a 3.5" separation distance between the extra magnets rather than a 3.1" distance because this dimension was changed without enough time to repeat the simulations. Figure 4-19a shows the magnetic field between the sputter guns without any additional magnets present. The field at the surface of the magnets is .03 tesla. We can see that the field strength ranges from .015 tesla to .03 tesla between the guns. This means that, according to Equation 2.6, the spiral radius of an electron traveling vertically

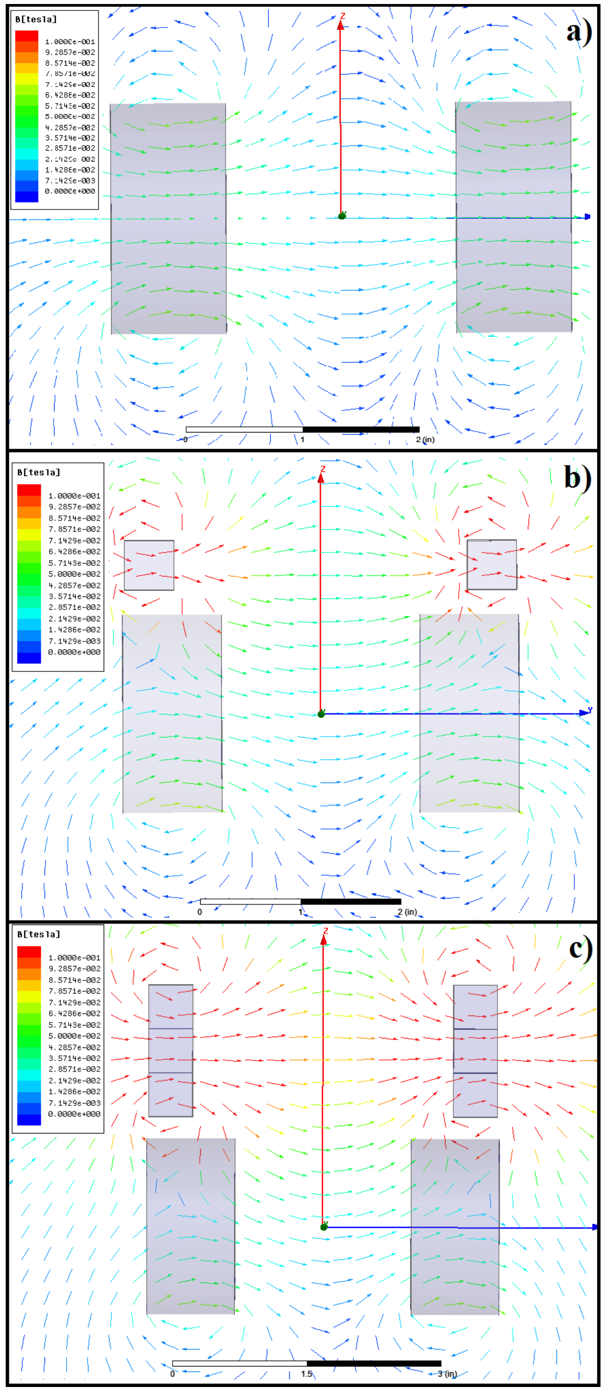

Figure 4-19: Magnetic field simulations conducted with Ansys Maxwell 3D as seen from the side. a) shows the magnetic field between the sputter guns with no additional magnets present, b) shows the field between the guns with two additional magnets present, and c) shows the field between the guns with 6 additional magnets present.

in this region with a kinetic energy of 500 eV would range from 0.25 cm to 0.5 cm. Given that the region between the targets is a 2" cube, this range of radii should be sufficient to effectively trap the electrons in this region. However, the field strength does fall off fairly quickly towards the top and bottom edges of the region between the targets, and significant fringing does occur, as expected.

Figure 4-19b shows that the addition of two extra magnets in the region above the sputter guns significantly increases the field strength and straightens the field lines near the target edges. The field at the surface of these magnets is .4871 tesla. We can see that, with this addition, the field between the targets is fairly constant around .015 tesla, and the field lines are horizontal throughout much of the region between the targets. Figure 4-19c shows the effect of six of these additional magnets. We can see the field generated by these magnets is significantly stronger than the one generated by only two magnets, with a value of .08 tesla at the midpoint between the stack of extra magnets. This field actually causes the field lines between the targets to bend downward. This effect will be discussed in Section 4.3.

Once the sputtering system is built, we will want to be able to vary the substrate-to-target distance in order to optimize the system. To achieve this, we included three stackable collar pieces of varying height, which allow five possible substrate-to-target distances. These are shown in Figure 4-17. The magnet holding apparatus also includes five stackable pieces, corresponding to the five collar pieces, so that as substrate-to-target distance increases, the width of the magnetic field between the substrates and the targets also increases. Because of this, we predict that substrate damage will decrease with substrate-to-target distance. Furthermore, this method might render the target shields proposed by Lei et. al. unnecessary, since it should negate the fringing effect at the edges of the magnetrons.

Figure 4-20: A set of three stackable "collar" pieces allow five possible substrate-to-target distances.

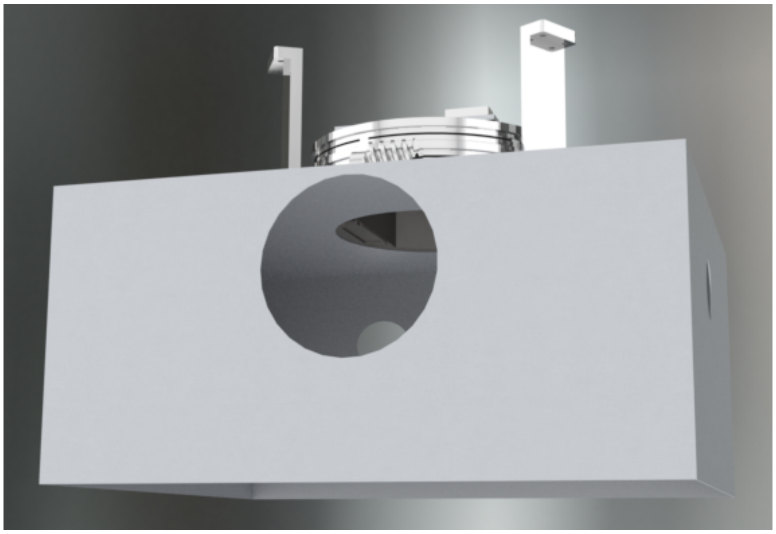

Figure 4-21: Solidworks representation of metal sleeve. As in the evaporator, the sleeve is suspended from the "hooks" in the substrate rotation mechanism.

Because of the varying collar heights, five different small sleeves are necessary to protect the chamber walls and rotation mechanism from vaporized material during deposition.

4.2.5 Metal sleeve

The sputtering system's metal sleeve is very similar to the evaporator's and serves the same purpose: to protect the chamber walls during deposition. It will also be suspended from the bottom of the hooks, as shown in Figure 4-21. Again, though all feedthroughs into the chamber must be removed in order to remove the sleeve, it provides a significant advantage over common cleaning processes.

4.2.6 Shutter

As in the evaporator, the shutter is located underneath the substrate rotation mechanism and is operated from outside the chamber using a feedthrough. Its purpose is to block the substrates from vaporized source material before and after desired deposition in order to ensure accurate layer thickness. The shutter for the sputtering system is yet to be designed, but we expect it to include two half-circular pieces which fit together underneath the substrate rotation mechanism. They will attach to a 90-degree-elbow shaft operated by a feedthrough in the base plate. When the feedthrough is rotated, the two half-circular pieces will rotate away from each other to allow vaporized material to coat the substrates.

4.2.7 Quartz crystal thickness monitor

The quartz crystal thickness monitor in the sputtering system is exactly the same device as in the evaporator. Its purpose is to measure the thickness of deposited films. Ideally we would have placed the thickness monitor above the shutter so that when the shutter closed, the deposition rate displayed by the thickness monitor would correspond accurately to the deposition rate on the substrates. However, there isn't room in this design because the magnetrons need to be so close to the substrates. Instead, we placed the thickness monitor below the magnetrons, which will work because the same amount of source material will diffuse downward as upward.

4.2.8 Vacuum system

The sputtering system will use the same backing and roughing pumps as the evaporator is currently using. It will also be equipped with a turbomolecular pump connected directly to the sputtering chamber. This vacuum system will operate in the same way as the evaporator's. The sputtering system, however, will include a variable gate valve between the mouth of the turbo and its chamber flange. This will allow us to raise the pressure in the chamber to begin operation by admitting argon through the gas inlet in the sputter gun heads.

4.3 Discussion

We expect the sputtering system to be built by the end of the summer. As yet, we have no price estimate for the completed system, and the design is subject to change before the system is built. However, since the sputtering chamber is fairly similar in volume to the evaporator and includes similar interior components, it is reasonable to assume that the pump-down time from atmospheric pressure to high vacuum will be similar to that of the evaporator. Deposition time will depend on deposition rate, which will in turn depend on the substrate-to-target distance and operating pressure we find to be most appropriate. Because the sputtering system includes the same number of feedthroughs as the evaporator, switching out a dirty metal sleeve for a clean one should also take about 15 minutes.

Once the system is complete we will test its low-damage capabilities, with and without the additional high strength magnets at varying substrate-to-target distances. To quantify substrate damage, we will fabricate OLEDs using materials similar to those used by studies cited in Section 4.1, and measure leakage current density at reverse bias of these devices. We will also measure photoluminescence intensity of a BAlq layer (as used by Lei et. al. and Onai et. al) or an Alq3 layer (as used by Yamada et. al) before and after deposition of an ITO electrode.

It should be noted that several sacrifices had to be made in order to incorporate low-damage technologies and multilayer deposition into the sputtering system design. For example, the sputtering chamber could have been smaller if we had used the planar sputtering configuration, and uniformity could have been improved using a method called off-axis sputtering, in which the sputter gun face is positioned at an angle to the substrates. The facing target configuration also required a custom gun design, which increased the total cost of the system.

The facing target configuration also poses an additional drawback: the vaporized material will diffuse out of the sides and bottom of the dense plasma region between the targets, as well as out of the top. This means that more source material will be wasted than would have been if we had used the planar sputtering configuration. However, we believe that these drawbacks will be justified if we succeed in reducing substrate damage.

The presence of the additional magnets near the sputter guns might also cause the target to erode non-uniformly over time. Strengthening the magnetic field and straightening the flux lines at the top edges of the dense plasma region between the targets may cause more charged particles to escape from the bottom of the dense plasma region than the top. This in turn may cause heavier ion bombardment at the top of the targets than the bottom, which will result in faster erosion of the material at the top of the targets. However, this shouldn't be a problem for several reasons. First, the target should erode more uniformly in the facing target configuration than the planar magnetron configuration in the first place [32]. The problematic erosion trenches present in the planar configuration are products of the E×B drift path caused by the perpendicular electric and magnetic fields. Since the electric and magnetic fields are parallel in the facing target configuration, these erosion trenches are not a problem. Second, the increased density of charged particles at the top of the dense plasma region will only increase target usage, albeit non-uniformly. Last, when the erosion at the top of the target becomes critical, a laboratory worker can simply rotate the targets manually between deposition runs to place the less eroded edge at the top of the dense plasma region.

In fact, this increase in erosion uniformity in the facing target configuration compared to the planar configuration may negate the material usage problem I mentioned earlier. If the amount of material that diffuses out of the sides and bottom of the dense plasma region in the facing target configura-

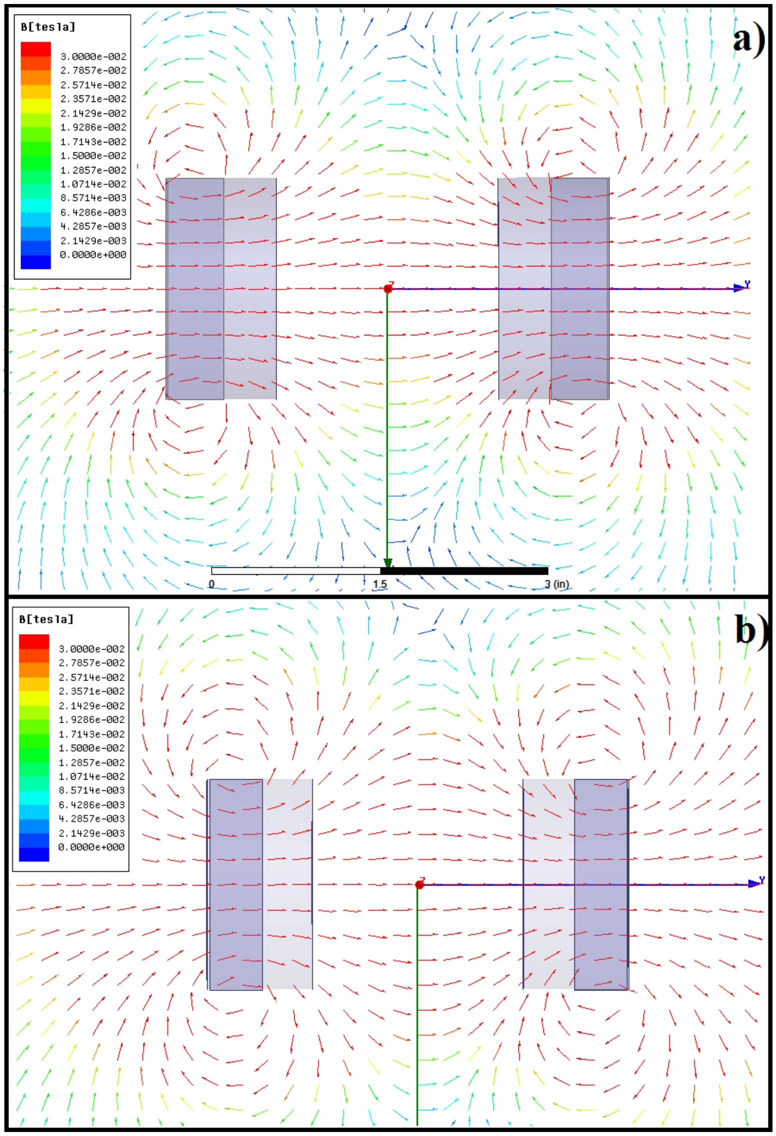

Figure 4-22: Simulations of the magnetic field between the additional magnets on a scale of zero to .03 tesla as seen from above. a) shows that, with two extra magnets present in the chamber, the magnetic field falls as low as 2.5×10^{-3} tesla towards the edges of the substrate rotation column, and b) shows that, with six extra magnets, the magnetic field falls to 6×10^{-3} tesla towards the edges of the substrate rotation mechanism.

tion is equal to the amount of material wasted by non-uniform erosion in the planar configuration, the material usage efficiency will be the same in the two configurations.

It should also be noted that, because the magnets are only 2” long, the additional magnetic field we have added in order to further reduce substrate damage decreases in strength towards the sides of the substrate rotation column. Figure 4-22 shows simulations of this magnetic field as seen from above. This may cause substrates at the edges of the substrate holder to be more susceptible to damage by energetic particles in the sputtering plasma than substrates at the center of the substrate holder. When testing this feature, we will simply place substrates only in the middle section of the substrate holder, so that they are protected by the strongest region of the extra magnetic field. If this feature turns out to protect substrates effectively, we will work on strengthening the magnetic field at the sides of the substrate rotation column.

As noted at the end of Section 4.2.4, an effect seen in Figure 4-19c should also be discussed. Looking back at this figure, we can see that when six extra magnets are present in the chamber, the field lines between the targets actually begin to bend downward, rather than remaining horizontal. This effect will have two consequences. First, it will increase the fringing at the bottom of the dense plasma region, which will increase the loss rate of charged particles from the bottom of this region. This in turn will enhance the non-uniform erosion pattern discussed above. Second, this reverse-fringing effect might also render the field between the targets less effective for confining charged particles. If the field lines are not entirely horizontal, the magnitude of the component of the field perpendicular to the velocity of an electron which is traveling vertically will decrease, which, in turn, will decrease the centripetal force on the electron. This is undesirable, since we are most concerned with confining the charged particles that are traveling vertically, i.e. in the direction of the substrates. These consequences suggest that it might be more effective to use weaker magnets in the region above the targets, which would also make our design more space efficient.

Assuming our low-damage feature does reduce substrate damage effectively, the method may be difficult to convert for use in large scale applications. Since the magnets must be so close together in order to generate a sufficiently strong field to trap electrons, the substrate width would be limited. This problem could likely be solved by lateral substrate motion. If not, the method is still worth investigation at a small scale, and large scale application can be addressed once the method is proven to be effective.

In accordance with the evaporator system flaws described in Section 3.4, we have improved certain aspects of the sputtering system with respect to the evaporator. First, we made the sputtering system's base plate one inch thicker than the evaporator's in order to avoid the warping problem experienced by the evaporator.

The sputtering design also includes two viewports instead of the evaporator's one, so that a laboratory worker can shine light into one while looking into the other. This will allow the laboratory worker to better see vaporized material in the chamber and confirm that the system is functioning properly. The primary viewport on the front of the chamber is also much bigger than the evaporator's viewport.

We are currently planning to attach the protective metal sleeve to the bottom of the "hooks" in the substrate rotation mechanism with magnets, which would make it easier for a laboratory worker to switch out sleeves. However, there is some worry that these magnets will interact undesirably with the magnets present in the chamber, so we might need to consider other attachment methods. The retractable base plate elevator mechanism is yet to be determined, but we are planning to implement a motorized or rack-and-pinion elevator system with a pneumatic system to catch the base plate when it falls open.

Since the sputtering system only requires two power supplies, it avoids the evaporator's problem with the large boat switch. We have also taken care to restrict the amount of space under the glove box used by the sputtering system, so there is plenty of room for an additional apparatus.

Chapter 5

Conclusion

Thin film technology is becoming increasingly important for the improvement of electronic semiconductor devices. If these devices are to continue to improve, it is clear that reliable thin film deposition processes are necessary.

In this project, we designed and constructed a state-of-the-art thermal evaporator which is inexpensive, simple and quick to operate, and easy to maintain. With all parts new, the total cost of the system is less than $40K. It takes under 3 minutes to bring the chamber from atmospheric pressure to operating pressure, and deposition takes under 10 minutes. Cleaning is as simple as switching out one internal protective metal sleeve for another, which takes 15 minutes at most. These improvements will provide research opportunities to individuals with less time and fewer resources, such as students working at undergraduate universities and liberal arts colleges.

We also designed a novel magnetron sputtering system which attempts to decrease damage inflicted upon substrates by high energy charged particles in the sputtering plasma. The facing target configuration has been shown by previous studies to confine the sputtering plasma below the substrates more effectively than the commonly used planar configuration. Sector-shaped target shields proposed by Li et. al. have also been shown to decrease impingement of high energy electrons on the substrates. Consequently, both of these methods are employed in our design.

We also added our own novel feature that we believe will further protect our substrates from energetic particle bombardment: an array of magnets in the sputtering chamber between the sputter guns and the substrates. Finite element simulations using Ansys Maxwell 3D showed that these magnets strengthen the magnetic field and reduce fringing near the top edges of the targets. We believe that, since this field extends beyond the plasma generation region, even particles that escape the region of dense plasma between the targets will be confined in some space. These magnets might even obviate the need for the target shields proposed by Lei et. al. Once the system is built, we will test its low-damage capabilities by measuring leakage current density of OLEDs at reverse bias and photoluminescence degradation of organic films during sputter deposition.

If this substrate protection apparatus proves effective, it could be modified for various marketable applications. For example, a sputter gun could be manufactured in which the area occupied by the magnets extends well beyond the target region. This would employ our apparatus's concept of extending the magnetic field beyond the plasma generation region in a simpler and possibly more effective design. Ultimately, we hope this project will facilitate the fabrication and research of high quality electronic devices with cutting-edge device architecture. If so, it could be a step towards ushering in a new generation of cheap electronics and possible renewable energy solutions.

Bibliography

[1] Kurt J. Lesker Company. Kurt J. Lesker Company. http://www.lesker.com/newweb/index.cfm. Accessed: 2013-04-15.

[2] Lawrence J. Overzet. The Plasma Applications Laboratory (PAL). http://www.utdallas.edu/~overzet/PALpict.htm, 1997. Accessed: 2013-04-15.

[3] Inc MBRAUN. MBRAUN. mbraunusa.com. Accessed: 2013-04-15.

[4] YouJong Lee, JooHyung Kim, Jin N. Jang, Ie H. Yang, SoonNam Kwon, MunPyo Hong, Dae C. Kim, Koung S. Oh, Suk J. Yoo, Bon J. Lee, and Won-Gun Jang. Development of inverted OLED with top ITO anode by plasma damage-free sputtering. *Thin Solid Films*, 517(14):4019–4022, May 2009.

[5] Minoru Yamada, Michio Matsumura, and Yasuhiro Maeda. Suppression of damage to organic light-emitting layers during deposition of Al-doped ZnO thin films by radio-frequency magnetron sputtering. *Thin Solid Films*, 519(10):3352–3357, March 2011.

[6] Hidetoshi Yamamoto, Takahito Oyamada, William Hale, Shoichi Aoshima, Hiroyuki Sasabe, and Chihaya Adachi. Low-Damage Indium Tin Oxide Formation on Organic Layers Using Unique Cylindrical Sputtering Module and Application in Transparent Organic Light-Emitting

Diodes. *Japanese Journal of Applied Physics*, 45:L213–L216, February 2006.

[7] Han K. Kim, D. G. Kim, K. S. Lee, M. S. Huh, S. H. Jeong, K. I. Kim, H. Kim, D. W. Han, and J. H. Kwon. Plasma damage-free deposition of Al cathode on organic light-emitting devices by using mirror shape target sputtering. *Applied Physics Letters*, 85(19):4295–4297, 2004.

[8] Jin-A Jeong, Han-Ki Kim, Jae-Young Lee, Jung-Hwan Lee, Hyo-Dae Bae, and Yoon-Heung Tak. Characteristics of ITO electrode grown by linear facing target sputtering with ladder type magnetic arrangement for organic light emitting diodes. *Thin Solid Films*, 517(14):4043–4046, May 2009.

[9] Hao Lei, Keisuke Ichikawa, Meihan Wang, Yoichi Hoshi, Takayuki Uchida, and Yutaka Sawada. Investigation of Low-Damage Sputter-Deposition of ITO Films on Organic Emission Layer. *The Institute of Electronics, Information, and Communication Engineers*, E91-C(10):1658–1662, October 2008.

[10] DongHyeok Lee, JinNyoung Jang, KwangHo Kwon, SukJae You, BonJu Lee, and MunPyo Hong. Influence of argon neutral beam energy on the structural properties of amorphous carbon thin films grown by neutral particle beam assisted sputtering. *Thin Solid Films*, 519(20):6703–6707, August 2011.

[11] Alexi C. Arango. *High open-circuit voltage in heterojunction photovoltaics containing a printed colloidal quantum-dot photosensitive layer*. PhD thesis, Massachusetts Institute of Technology, 2010.

[12] Jong-Min Moon and Han-Ki Kim. Sputtering of Aluminum Cathodes on OLEDs Using Linear Facing Target Sputtering with Ladder-Type Magnet

Arrays. *Journal of the Electrochemical Society*, 155(7):J187–J192, March 2008.

[13] Werner Kern. *Thin Film Processes, Volume 2 (Pt. 2)*. Academic Press, May 1991.

[14] P. J. Kelly and R. D. Arnell. Magnetron sputtering: a review of recent developments and applications. *Vacuum*, 56(3):159–172, March 2000.

[15]

[16] Joo H. Kim, You J. Lee, Yoon S. Jang, Jin N. Jang, Doo H. Kim, Byung C. Song, Dong H. Lee, Soon N. Kwon, and MunPyo Hong. The effect of Ar plasma bombardment upon physical property of tungsten oxide thin film in inverted top-emitting organic light-emitting diodes. *Organic Electronics*, 12(2):285–290, February 2011.

[17] *A User's Guide to Vacuum Technology 2nd edition by O'Hanlon, John F. published by Wiley-Interscience Hardcover*. Wiley-Interscience, April 1989.

[18] Donald Smith. *Thin-Film Deposition: Principles and Practice*. McGraw-Hill Professional, 1 edition, March 1995.

[19] Yoichi Hoshi and Takakazu Kiyomura. ITO thin films deposited at low temperatures using a kinetic energy controlled sputter-deposition technique. *Thin Solid Films*, 411(1):36–41, May 2002.

[20] Y. Hoshi, E. Suzuki, and H. Shimizu. Control of crystal orientation of Ti thin films by sputtering. *Electrochimica Acta*, 44(21-22):3945–3952, June 1999.

[21] S. Dangtip, Y. Hoshi, Y. Kasahara, Y. Onai, T. Osotchan, Y. Sawada, and T. Uchida. Study of low power deposition of ITO for top emission

OLED with facing target and RF sputtering systems. *Journal of Physics: Conference Series*, 100(4):042011+, March 2008.

[22] Yusuke Onai, Takayuki Uchida, Yoshihiro Kasahara, Keisuke Ichikawa, and Yoichi Hoshi. Transparent conductive film for top-emission organic light-emitting devices by low damage facing target sputtering. *Thin Solid Films*, 516(17):5911–5915, July 2008.

[23] Xin-Shan Li, Kaoru Yamashita, Tsunehisa Tanaka, Yoshihiko Suzuki, and Masanori Okuyama. Structural and electrical properties of highly oriented Pb(Zr,Ti)O3 thin films deposited by facing target sputtering. *Sensors and Actuators A: Physical*, 82(1-3):265–269, May 2000.

[24] M. Swarnalatha and S. Mohan. Twin facing target sputtering system for the deposition of multilayer and alloy films. *Vacuum*, 48(1):15–19, January 1997.

[25] Xin-Shan Li, Tsunehisa Tanaka, and Yoshihiko Suzuki. Characterization of lead zirconate titanate thin films deposited at low temperature by reactive facing target sputtering. *Thin Solid Films*, 375(1-2):267–270, October 2000.

[26] Morito Matsuoka, Yoichi Hoshi, and Masahiko Naoe. rf and dc discharge characteristics for opposed-targets sputtering. *Journal of Applied Physics*, 60(6):2096–2102, 1986.

[27] Han K. Kim, D. G. Kim, K. S. Lee, M. S. Huh, S. H. Jeong, K. I. Kim, and Tae Y. Seong. Plasma damage-free sputtering of indium tin oxide cathode layers for top-emitting organic light-emitting diodes. *Applied Physics Letters*, 86(18):183503+, 2005.

[28] Han K. Kim, Sang W. Kim, Kyu S. Lee, and K. H. Kim. Direct Al cathode layer sputtering on LiF/Alq[sub 3] using facing target sputtering

with a mixture of Ar and Kr. *Applied Physics Letters*, 88(8):083513+, 2006.

[29] Jin-A Jeong, Han-Ki Kim, and Seok-In Na. Low Resistance and High Transparent Amorphous IZTO Electrode Cosputtered by Linear Facing Target Sputtering for Organic Photovoltaics. *Electrochemical and Solid-State Letters*, 12(9):J80–J82, June 2009.

[30] Kwang-Hyuk Choi, Jin-A Jeong, and Han-Ki Kim. Dependence of electrical, optical, and structural properties on the thickness of IZTO thin films grown by linear facing target sputtering for organic solar cells. *Solar Energy Materials and Solar Cells*, 94(10):1822–1830, October 2010.

[31] Jin-A Jeong, Han-Ki Kim, and Seok-In Na. Low Resistance and High Transparent Amorphous IZTO Electrode Cosputtered by Linear Facing Target Sputtering for Organic Photovoltaics. *Electrochemical and Solid-State Letters*, 12(9):J80–J82, June 2009.

[32] Qihua Fan. Uniformity of targets erosion and magnetic film thickness distribution in the target-facing-type sputtering method. *Journal of Vacuum Science & Technology A: Vacuum, Surfaces, and Films*, 10(5):3371–3375, September 1992.